Available online at www.sciencedirect.com
ScienceDirect
Geochimica et Cosmochimica Acta 75 (2011) 4194–4215
Geochimica et Cosmochimica Acta
www.elsevier.com/locate/gca

# Environmental memory and a possible seasonal bias in the stable isotope composition of (U–Th)/He-dated goethite from the Canadian Arctic

Crayton J. Yapp [a,*], David L. Shuster [b,c]

[a] Huffington Department of Earth Sciences, Southern Methodist University, Dallas, TX 75275-0395, United States
[b] Berkeley Geochronology Center, 2455 Ridge Road, Berkeley, CA 94709, United States
[c] Department of Earth and Planetary Science, University of California, Berkeley, CA 94720, United States

Received 26 August 2010; accepted in revised form 27 April 2011; available online 5 May 2011

**Abstract**

Goethite (Ax-2) from Axel Heiberg Island (~80°N) on the margin of the Arctic Ocean is the dominant mineral in a sample of "petrified" Eocene wood, but U, Th, and He measurements suggest that the goethite (α-FeOOH) crystallized in the latest Miocene/Pliocene (ca. 5.5 to 2.8 Ma). Measured δD and $\delta^{18}O$ values of Ax-2 are −221 (±6)‰ and −9.6 (±0.5)‰, respectively. The inferred δD and $\delta^{18}O$ values of the ancient water were about −139‰ and −18.6‰, respectively, with a calculated temperature of crystallization of 3 (±5)°C, which compares with the modern summer (J-J-A) temperature of 3 °C and contrasts with a modern MAT of −19 °C. Published results from various biological proxies on nearby Ellesmere Island indicate a Pliocene (~4 Ma) MAT of either −6 or −0.4 °C and corresponding seasonal amplitudes of about 18 or 13 °C. A conductive heat flow model suggests that a temperature of 3 °C could represent goethite crystallization at depths of ~100–200 cm (for MAT = −6 °C) or ~250–450 cm (for MAT = −0.4 °C) over seasonally restricted intervals of time.

The $\delta^{18}O$ value of the Ax-2 water (−18.6‰) is more positive than the modern J-J-A precipitation (−22‰). In combination, the paleotemperatures and $\delta^{18}O$ values of ancient waters (from Ax-2 and published results from three Eocene or Pliocene proxy sites on Axel Heiberg and Ellesmere Islands) are consistent with a warm season bias in those isotopic proxies. The results are also consistent with higher proportions of J-J-A precipitation in the annual total. If so, this emphasizes the importance of seasonality at high latitudes even in times of warmer global climates, and suggests that the Arctic hydrologic cycle, as expressed in the seasonal distribution and isotopic composition of precipitation (perhaps modified by a warmer Arctic Ocean), differed from modern.

The $\delta^{13}C$ value of the $Fe(CO_3)OH$ component in the Ax-2 goethite is +6.6‰, which is much more positive than expected if crystallizing goethite incorporated $CO_2$ derived primarily from oxidation of relict Eocene wood with $\delta^{13}C$ values of about −24‰. This apparent paradox may be resolved if the goethite is a product of oxidation of $^{13}C$-rich siderite, which had previously replaced wood in an Eocene methanogenic burial environment. Thus, the goethite retains a carbon isotope "memory" of a diagenetic Eocene event, but a δD and $\delta^{18}O$ record of the latest Miocene/Pliocene Arctic climate.


## 1. INTRODUCTION

Studies of the stable oxygen and/or hydrogen isotope composition of the common mineral goethite (α-FeOOH) can provide information on temperatures and meteoric waters in a variety of oxidizing environments (Yapp, 1987a, 1993, 1997, 1998, 2000, 2008; Bird et al., 1992, 1993; Hein et al., 1994; Girard et al., 1997, 2000, 2002; Bao et al., 2000; Pack et al., 2000; Poage et al., 2000; Sjostrom et al., 2004; Tabor et al., 2004a; Fifarek and Rye, 2005; Seidel et al., 2005; Tabor and Yapp, 2005; Hren et al., 2006; Grosz et al., 2006; Dideriksen et al., 2010). For many of these studies, the age of the goethite samples was constrained by the stratigraphy of the host deposits and the textural relation of the goethite to that host

* Corresponding author.
*E-mail address:* cjyapp@smu.edu (C.J. Yapp).

0016-7037/$ - see front matter © 2011 Elsevier Ltd. All rights reserved.
doi:10.1016/j.gca.2011.04.029

material. In two instances of Holocene-age material, ages were constrained by $^{14}C$ dating of wood embedded in successions of iron oxide deposits (Poage et al., 2000; Sjostrom et al., 2004). However, for some of the studied systems, goethite was a secondary mineral in the host material and the age of crystallization of the goethite remained uncertain. The value of paleoenvironmental information obtained from oxygen and hydrogen isotope data in such goethite systems would be greatly enhanced if credible information on the antiquity of the goethite were available.

Lippolt et al. (1998) showed that (U–Th)/He dating techniques applied to natural goethites yielded a variety of ancient ages of crystallization, but they noted that partial loss of $^4He$ by diffusion and/or α-particle ejection would result in underestimates of the ages. Shuster et al. (2005) demonstrated that the partial loss of $^4He$ by diffusion could be taken into account by first subjecting natural goethite samples to proton irradiation that produced spallogenic $^3He$, which was uniformly distributed in the irradiated samples. Measurement of incremental loss of $^3He$ during stepwise heating of the irradiated samples was used to determine the temperature-dependent magnitude of domain-normalized He diffusion coefficients ($D/a^2$; see Shuster et al., 2005, for details). Heim et al. (2006) successfully applied the (U–Th)/He technique to the dating of goethites in Miocene-age iron ore deposits in Australia.

Herein, we present results of the first study to combine stable hydrogen, carbon, and oxygen isotope measurements with (U–Th)/He dating of natural goethite. The paleosol-hosted sample from Axel Heiberg Island (~80°N latitude) is the most northerly occurrence of goethite known to the authors. At present, this Arctic location represents a rather extreme climatic environment, but the data from the diagenetic goethite provide information about the more moderate late Miocene/Pliocene environmental conditions that existed prior to the onset of Pleistocene-style glaciation in the northern hemisphere. The degree of seasonality in the Pliocene Arctic was apparently smaller than in the Holocene (e.g., Elias and Matthews, 2002; Haywood et al., 2009; Ballantyne et al., 2010a) but significant enough to suggest that a seasonal bias in the D/H and $^{18}O/^{16}O$ ratios of the goethite might be identified. Climatic implications of these data are discussed in the context of other Tertiary isotopic proxies in the Arctic. The goethite also preserves some isotopic information from a reducing, diagenetic system that preceded the late Miocene/Pliocene oxidizing environment in which the goethite crystallized. Local carbon cycling associated with this change in diagenetic conditions is discussed in terms of the carbon isotope composition of the $Fe(CO_3)OH$ component in the goethite. The results illustrate not only the promise of the combined isotopic approach as applied to diagenetic goethite but also its potential analytical and conceptual complexities.

## 2. SAMPLE AND ANALYTICAL METHODS

### 2.1. Sample location

The material (designated Ax-2) was provided by Dr. Hope Jahren who collected it from an outcrop of what was a podzolic soil during the middle Eocene. The paleosol was in a layer between the coal of the A′ and B′ layers of the middle Eocene age (~45 Ma) Buchanan Lake Formation on Axel Heiberg Island, Canada (e.g., Jahren and Sternberg, 2002; Jahren et al., 2009). At this location (79°55′ N, 89°02′ W), portions of the Buchanan Lake Formation contain well-preserved, cellulose-bearing wood from a middle Eocene forest hosted by alluvial sediments comprised of mudstones, claystones, sandstones, organic-rich shale, and lignite (e.g., Jahren and Sternberg, 2002; Jahren, 2007; Jahren et al., 2009). The location of Ax-2 on Axel Heiberg Island and the locations of two nearby IAEA stations (at Eureka and Alert on Ellesmere Island) are indicated in Fig. 1.

### 2.2. Sample characterization

Sample characterization was performed in the Huffington Department of Earth Sciences at Southern Methodist University (SMU) with thin section petrography, scanning electron microscopy (SEM, using a Leo 1450VPSE), and X-ray powder diffractometry (XRD, using a Rigaku Ultima III with Cu-$K_\alpha$ radiation). At hand sample (Fig. 2a) and thin section (Fig. 2b) scales, Ax-2 exhibits the textural features of fossil wood. However, the concentration of $H_2O_2$-oxidizable organic carbon is only 0.8 wt.% (method of Yapp and Poths, 1991).

The XRD spectrum of Fig. 3 indicates that Ax-2 is comprised predominantly of goethite (α-FeOOH) with accessory hematite (α-$Fe_2O_3$) and some minor lepidocrocite (γ-FeOOH). No other minerals are detectable by XRD. In addition, the XRD method of Schulze (1984) shows no evidence of substitution of Al for Fe in the goethite structure.

### 2.3. Stable isotope analyses

Prior to stable isotope analysis, approximately 3 g of Ax-2 was powdered under reagent-grade acetone in an aluminum oxide mortar and pestle. The powder was passed through a cleaned brass sieve with a mesh of 63 μm. This <63 μm powder was treated for ~16 h at room temperature (22 °C) with 0.5 M HCl, then thoroughly rinsed with de-ionized water. The rinse was considered complete when the pH of the rinse water did not change from its initial value of ~5.5 after 10 min of continuous contact with the sample. This was followed by treatment with at least four successive aliquots of ~30% $H_2O_2$ solution at room temperature for a total of 30 days (Yapp and Poths, 1991; Yapp, 1998). After decanting the last aliquot of $H_2O_2$, the sample was dried in a vacuum desiccator at room temperature with no additional rinsing with de-ionized water. The overall procedure is intended to provide a "cleaned", relatively large, reasonably well-mixed sample to optimize stable isotope homogeneity among the different aliquots that were subsequently analyzed.

#### *2.3.1. Hydrogen isotope analyses*

After outgassing in vacuum for 60 min at 100 °C (Yapp and Pedley, 1985), the goethite of Ax-2 still contained a large proportion of exchangeable hydrogen. This exchangeable

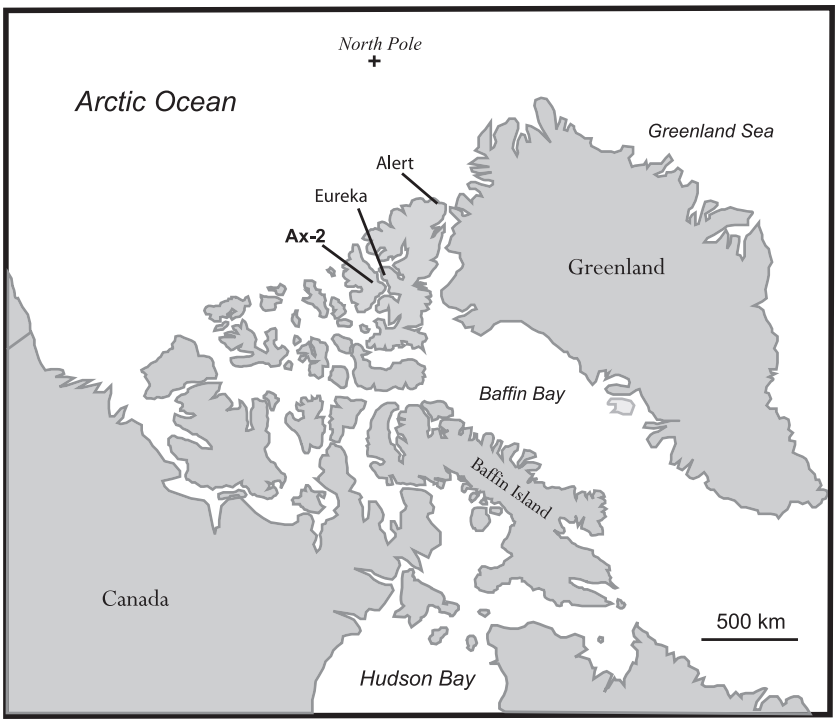


Fig. 1. Site locations of goethite sample Ax-2 (79°55′N, 89°02′W) on Axel Heiberg Island and the two IAEA/WMO precipitation stations, Alert (82.3°N, 62.2°W) and Eureka (80.0°N, 85.56°W), on Ellesmere Island in the Canadian Arctic on the margin of the Arctic Ocean.

hydrogen is referred to as "high temperature non-stoichiometric" (HTN) hydrogen and rapidly exchanges D/H with ambient vapor at 22 °C (Yapp and Poths, 1995). Consequently, mineral-vapor hydrogen isotope exchange experiments were performed to obtain the D/H ratio of non-exchangeable structural hydrogen in Ax-2 goethite (Yapp and Poths, 1995; Feng and Yapp, 2008).

For these experiments, an aliquot of the sample was outgassed in vacuum at 100 °C for 60 min, then cooled under vacuum to 22 °C, followed by D/H exchange for 18 h at 22 °C with a measured amount of water vapor with a known initial δD value. At the end of this time, the 22 °C exchange experiment was "quenched" by freezing the water vapor into a liquid nitrogen-cooled multiple coil trap, and the sample was further outgassed at 100 °C for an additional 60 min while still open to the cold trap. This "exchanged" water vapor was passed through a depleted uranium furnace at ~760 °C and quantitatively converted to hydrogen gas. A Toepler pump was used to collect and measure the quantity of $H_2$ gas. The $H_2$ was subsequently transferred to a Finnigan 252, dual-inlet, isotope ratio mass spectrometer for measurement of its δD value. The sample of Ax-2 remaining in the dehydration chamber was heated at 850 °C for 30 min (converting the goethite to hematite) with the evolved water collected and analyzed for yield and δD value in the usual manner (see Yapp and Poths, 1995; Feng and Yapp, 2008, for details).

The manometrically measured hydrogen yields have a precision of ±1 μmol. The δD values are reported relative to the V-SMOW standard (hereafter referred to as SMOW) and have an analytical precision of ±1‰ for individual gas samples. All of the hydrogen isotope experiments and measurements were performed at SMU.

### 2.3.2. Oxygen isotope analyses

After loading into nickel reaction vessels and outgassing in vacuum at 22 °C for 60 min, aliquots of Ax-2 were pre-treated with ~0.05–0.17 bar of $BrF_5$ at 22 °C for various lengths of time (Yapp, 1987a). The reaction products from this pre-treatment were removed, and the residual sample was reacted with ~7-fold excess of $BrF_5$ at 450 °C for ~14 h (Clayton and Mayeda, 1963). $O_2$ recovered as a product of the 450 °C reaction was quantitatively converted to $CO_2$ over a heated, spectroscopically pure carbon rod, and $CO_2$ yield was measured in an Hg manometer with a precision of ±1 μmol. The $\delta^{18}O$ value of the $CO_2$ was measured on a Finnigan 252 isotope ratio mass spectrometer with values reported relative to SMOW. Analytical precision is ±0.2‰. All of the oxygen isotope measurements were performed at SMU.

### 2.3.3. Carbon isotope analyses

Following outgassing at 100 °C in vacuum for 60 min, aliquots of Ax-2 were subjected to thermally driven dehydration-decarbonation to extract water and small amounts of co-evolved $CO_2$ from the goethite. The method used was that of Yapp and Poths (1991, 1993), as modified by Hsieh and Yapp (1999), with the collection of discrete increments of evolved gas (see the cited works for details). The $CO_2$ of interest is present in small concentrations as $Fe(CO_3)OH$ in solid solution in the goethite (e.g., Yapp, 1987b; Yapp and Poths, 1990). Increments of co-evolved $CO_2$ and water were

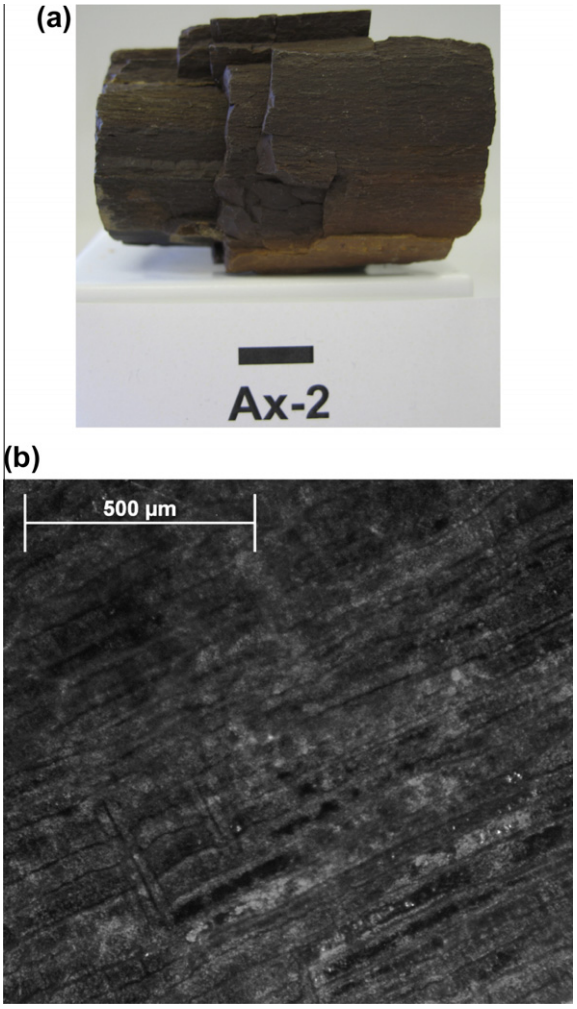


Fig. 2. (a) Photograph of Ax-2. Scale bar = 1 cm. (b) Photomicrograph of Ax-2 (plane polarized light) showing the preserved textures of the replaced Eocene wood.

separated cryogenically with a dry ice-methanol bath. The $CO_2$ was transferred to a small-sample Hg manometer for measurement of yield to precisions of ±0.1 μmol and then analyzed for its $\delta^{13}C$ value on a Finnigan 252 isotope ratio mass spectrometer. Values of $\delta^{13}C$ are reported on the V-PDB scale (hereafter termed PDB). Evolved water was converted to hydrogen gas as described previously with measurement of its yield to ±1 μmol. Analytical precision for $\delta^{13}C$ values of individual increments of $CO_2$ gas was ±0.3‰ for samples <~1.0 μmol and ±0.1–0.2‰ for samples >1.0 μmol. All of these analyses were performed at SMU.

### 2.4. (U–Th)/He analyses

As part of this effort, an aliquot of Ax-2 was exposed to ~$4.6 \times 10^{15}$ protons/cm$^2$ with incident energy ~220 MeV over a continuous 8 h period at The Francis H. Burr Proton Therapy Center to generate spallogenic $^3$He. Evolution of $^3$He during non-isothermal, stepwise heating experiments is used to determine values of $D/a^2$ over the range of temperatures (~140–250 °C) at which diffusive loss of He from the high retentivity domain (HRD) of goethite can be effectively measured (Shuster et al., 2005). "D" is the diffusion coefficient for He in goethite, and "a" is the dimension of the diffusion domain. However, for Ax-2, the breakdown of goethite to hematite began, in vacuum, at the low temperature of ~150 °C, which precluded determination of a credible Arrhenius relation for He diffusion in this goethite.

Discrete pieces of Ax-2 were micro-sampled (Table 1) and analyzed to determine the concentrations of U, Th, and He (e.g., Shuster et al., 2005). Concentrations of He were measured by mass spectrometry at the Berkeley Geochronology Center and those of U and Th at the California Institute of Technology in the laboratory of Dr. Kenneth Farley. Helium was recovered from sample aliquots by laser extraction. Relative analytical errors for the sample sizes of this study are typically ±2% of the nominal value.

## 3. RESULTS AND DISCUSSION

### 3.1. Age of crystallization

Environmental information obtained from the stable isotope composition is of limited use unless the age of Ax-2 goethite can be determined. The replacement texture (Fig. 2a and b) indicates that Ax-2 is younger than the Eocene wood, but it provides no information on the specific age of crystallization of the goethite. The (U–Th)/He chronometer (e.g., Shuster et al., 2005) was used to constrain this crystallization age.

Measured concentrations of U, Th, and He in six aliquots of Ax-2 are in Table 1. Detailed discussions of the (U–Th)/He method applied to minerals such as apatite and goethite are presented elsewhere (e.g., Lippolt et al., 1998; Wolf et al., 1998; Shuster and Farley, 2004, 2005; Shuster et al., 2005). With assumptions of closed system, secular equilibrium, no initial $^4$He, and time scales of less than ~300 Ma, the (U–Th)/He age equation can be expressed as follows (e.g., Wolf et al., 1998).

$$t' \approx \frac{[^4\mathrm{He}]}{8[^{238}\mathrm{U}]\lambda_{238} + 6[^{232}\mathrm{Th}]\lambda_{232}} \quad (1)$$

[$^4$He], [$^{238}$U], and [$^{232}$Th] are the measured concentrations of the indicated isotopes. $\lambda_{238}$ and $\lambda_{232}$ are the corresponding decay constants, and $t'$ is the nominal age calculated using Eq. (1). Eq. (1) is relevant to the current work, because Ax-2 is a secondary, authigenic mineral in a middle Eocene sedimentary deposit. Therefore, its age is <~45 Ma. The concentration of $^{235}$U does not appear in Eq. (1), because on the applicable time scale, the small value of the $^{235}$U/$^{238}$U ratio implies that the $^4$He contributed by $^{235}$U is less than 0.5% of that produced by decay of $^{238}$U (Wolf et al., 1998). Thus, to a first approximation, the concentrations of the isotopes in Eq. (1) can be considered to be the same as the total concentrations measured for those elements in Ax-2 (Table 1).

The calculated ages ($t'$) are in Table 1 and range from 0.6 to 5.5 Ma with a mean of 3.0 (±2.1) Ma. There appear to be three sets of approximately paired ages in Table 1 with respective average values of 5.4 (±0.2), 2.8 (±0.1), and 0.8 (±0.2) Ma. This range of ages may indicate that the

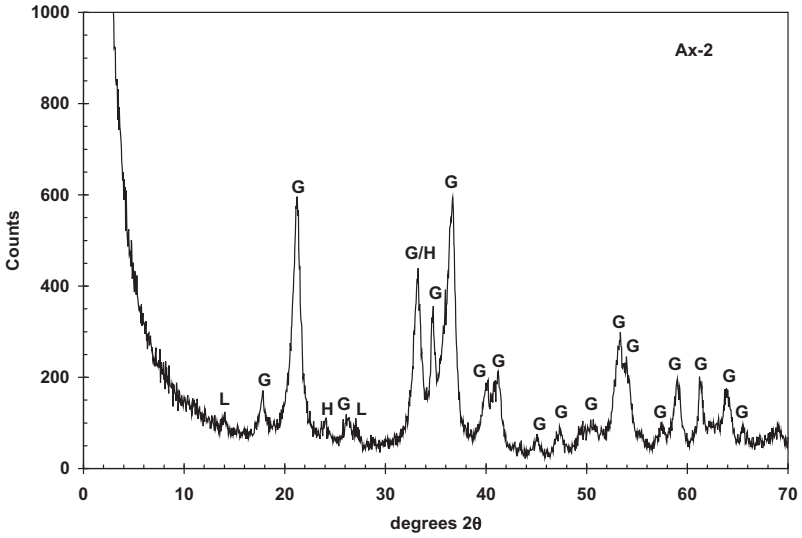


Fig. 3. XRD spectrum of Ax-2 using Cu-$K_\alpha$ radiation. G = goethite peaks. H = hematite peaks. L = lepidocrocite peaks. Goethite is the dominant mineral in the sample. There is no XRD evidence of substitution of Al for Fe in the goethite.

crystallization of Ax-2 goethite occurred more or less continuously over an interval from the latest Miocene well into the Pleistocene (Lugowski et al., 2009). Conversely, the different nominal ages might represent more episodic crystallization of Ax-2 over that interval. However, because of the possible diffusive loss of He and the presence of a low retentivity domain (LRD) in goethite (Shuster et al., 2005), each age in Table 1 represents a minimum age of crystallization for that aliquot.

As mentioned, the relatively low temperature (~150 °C) of the goethite to hematite phase transition in Ax-2 stymied determination of a credible Arrhenius relation for He diffusion coefficients in the goethite using stepwise heating in vacuum. However, Arrhenius relations for other goethites were used to estimate a value of $D/a^2$ at 3 °C (this temperature is justified in a subsequent section). Newly determined values of the activation energies ($E_A$) and pre-exponential factors [$\log_{10}(D/a^2)_0$] for He diffusion in goethite samples designated Roraima Territory and PPColo-2 are presented in Table 2. The implications of the results are discussed below. Also in Table 2 are values for two goethites published by Shuster et al. (2005). The values of $E_A$ and $\log(D/a^2)_0$ in Table 2 were used to calculate curves of $\log(D/a^2)$ vs. $10^4/T$, which are plotted in Fig. 4a. The applicability of the extrapolated curves of Fig. 4a to diffusion of He in Ax-2 at a temperature of 3 °C may be problematic, but these are the only values of $D/a^2$ currently available.

The curves of Fig. 4a diverge at low temperature (most notably the curve for PPColo-2). Consequently, they provide no evidence of a "consensus" value for $D/a^2$ in goethite at 3 °C. However, the more closely grouped lines representing the Roraima Territory, the BAH-F124-111.2, and the BAH-F124-114 samples in Fig. 4a may provide a rough indication of the overall uncertainty associated with determination of values of $D/a^2$ in many natural goethites. This possibility is reinforced by the fact that the Arrhenius curve for $D/a^2$ in PPColo-2 (Fig. 4a) is distinctly different from

Table 1
U–Th–He data and nominal ages of aliquots of Ax-2.

| Sample | Lab ref. # | Sample mass (μg) | Nominal[a] age (Ma) | U (nmol/g)[b] | Th (nmol/g)[b] | $^4$He (nmol/g)[b] | $^4$He extraction (method) |
|---|---|---|---|---|---|---|---|
| Ax-2x | 08APH | 34.8 | 2.8 | 1.4 | 4.2 | 0.0085 | Laser |
| Ax-2y | 08APQ | 42.0 | 2.8 | 1.2 | 4.4 | 0.0081 | Laser |
| AX-2-D | 08BSJ | 27.2 | 5.5 | 1.3 | 6.9 | 0.0204 | Laser |
| AX-2-E | 08BSN | 35.1 | 5.2 | 1.7 | 5.6 | 0.0201 | Laser |
| Ax-2 | 08AOY | 33.0 | 0.6 | 3.5 | 32.8 | 0.0092 | Laser |
| AX-2-F | 08BSR | 1.8 | 0.9 | 19.5 | 111.5 | 0.0600 | Laser |
| Average age: | | | 3.0 (±2.1)[c] | | | | |

[a] The nominal age is not corrected for $^4$He loss.
[b] The typical analytical uncertainty of individual measurements of U, Th, and He for aliquots of the size analyzed here is ~±2% of the nominal concentration. This uncertainty is much less than that associated with the scatter of the nominal calculated ages. Thus, the analytical uncertainty of the measured concentrations is not a significant factor in that scatter.
[c] The error shown for the average nominal age is one standard deviation.

Table 2
Arrhenius activation energies and pre-exponential factors for He diffusion in various goethites.

| Sample | $E_A$ (kJ/mol) | $\log_{10}(D/a^2)_0$ ($D/a^2$ in $s^{-1}$) |
|---|---|---|
| Roraima Territory[a] | 230 | 19.5 |
| PPColo-2[a] | 315 | 24.8 |
| BAH-F124-111.2[b] | 178.4 | 12.3 |
| BAH-F124-114[b] | 162.8 | 11.3 |

[a] This work.
[b] From Shuster et al. (2005).

(and generally lower than) the other three curves. PPColo-2 is a dense, coarsely crystalline goethite, for which one might expect the observed lower values of $D/a^2$. Some of the implications of the uncertainty about $D/a^2$ values in Ax-2 may be addressed with a published, isothermal, $^4$He production-diffusion model that is applicable for times of $<\sim$300 Ma (e.g., Wolf et al., 1998).

In addition to model assumptions discussed by Wolf et al. (1998), the current work incorporates the assumptions that (1) there was no $^4$He in the sample at the time of crystallization, and (2) Ax-2 has remained at a temperature of 3 °C since the time of crystallization. If the latter assumption were incorrect, it could be because Ax-2 resided, for part of its post-crystallization history, at even lower temperatures as the climate cooled into the Pleistocene. This would imply lower time-averaged values of $D/a^2$. The following "ingrowth-diffusion" equation expresses the relationship between the actual and nominal ages of crystallization under these conditions (e.g., Wolf et al., 1998):

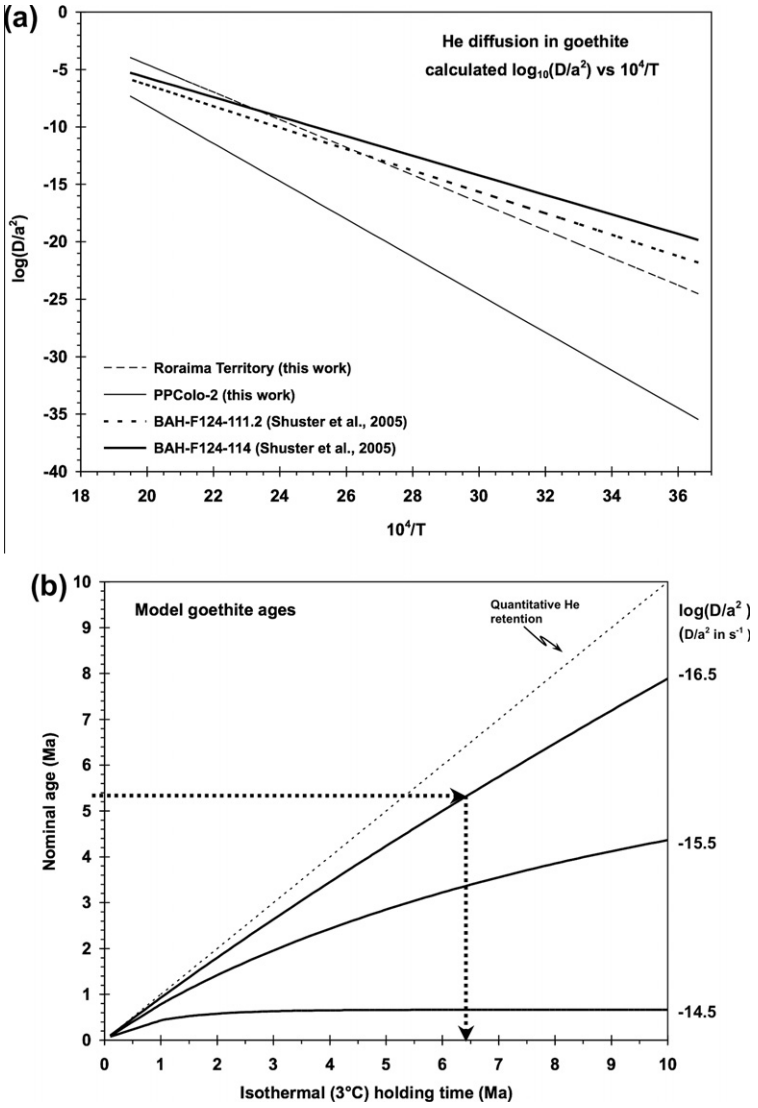


Fig. 4. (a) Values of $\log(D/a^2)$ for He diffusion in goethite plotted against $10^4/T$ (see text). (b) Model He production-diffusion curves (e.g., Wolf et al., 1998), which relate the nominal age of a sample (determined from measured values of the U, Th, and He concentrations) to the "isothermal holding time" at 3 °C. The sequential dashed arrows indicate that for a $\log(D/a^2)$ value of −16.5, the measured (nominal) age of 5.4 Ma represents a model isothermal holding age of ~6.5 Ma. See text.

$$t' = \frac{a^2}{D}\left[\frac{1}{15} - \sum_{n=1}^{\infty}\frac{6}{\pi^4 n^4}\exp\left(-n^2\pi^2\frac{D}{a^2}t\right)\right] \quad (2)$$

$t$ = the "isothermal holding time" (Wolf et al., 1998). For the assumptions applied to Ax-2, the isothermal holding time is the actual amount of time that has passed since the crystallization of the sample. $n = 1, 2, 3, \ldots$ etc. Other terms are as previously defined. From Eq. (2), model curves depicting the variation of nominal age ($t'$) with isothermal holding time ($t$) for different choices of $\log(D/a^2)$ were calculated and are plotted in Fig. 4b.

To make a substantial allowance for uncertainty about the value of $D/a^2$ and to err on the side of greater He loss (i.e., nominal sample ages possibly too young), it was assumed that $D/a^2$ for He in Ax-2 goethite at 3 °C was three orders of magnitude larger than the largest value at 3 °C in Fig. 4a [$\log(D/a^2) = -19.5$ for BAH-F124-114 at 3 °C]. Thus, a $\log(D/a^2)$ value of −16.5 was adopted for Ax-2 ($D/a^2$ in units of $s^{-1}$).

The average value (~5.4 Ma) of the two oldest ages of Table 1, when applied to the curve for $\log(D/a^2) = -16.5$ in Fig. 4b, indicates an isothermal holding time of ~6.5 Ma. This possible isothermal holding age does not take into account the likely existence of a low retentivity domain (LRD) for He in Ax-2 goethite. Shuster et al. (2005) found that the presence of an LRD resulted in an additional ~4% underestimate of the crystallization age of their sample BAH-F124-114 and an ~8% underestimate for BAH-F124-111.2. To make allowance for lack of knowledge of the magnitude of any LRD in Ax-2, we considered two progressively more extreme examples, (1) an LRD in Ax-2 that resulted in an additional 20% underestimate, which would yield a "corrected" Ax-2 age of ~8.1 Ma, or (2) a 40% LRD-induced underestimate, which would imply a corrected age of ~10.8 Ma. We have no evidence that such large LRD effects were operative in Ax-2, but even if the largest of these hypothetical LRD effects were applicable, it would still imply that the Ax-2 goethite had begun to crystallize in the latter half of the Miocene (e.g., Lugowski et al., 2009). To facilitate discussion, and in the absence of information to the contrary, it is assumed that the nominal ages ranging from 2.8 to 5.5 Ma in Table 1 may be reasonable estimates of the ages of crystallization. The meaning of the nominal ages of ~0.6 and 0.9 Ma (Table 1) is discussed in Section 3.4.2 in the context of the D/H and $^{18}O/^{16}O$ ratios, the U and Th concentrations, and the texture of the Ax-2 sample.

As mentioned, the different nominal ages in Table 1 (~2.8 and ~5.4 Ma) suggest the possibility that the goethite of Ax-2 did not form continuously throughout the Pliocene. Instead, the different ages may reflect more episodic crystal growth during that time. At present, we cannot distinguish between these possibilities.

### 3.2. Hydrogen isotopes

Results of the 22 °C mineral-vapor D/H exchange experiments are in Table 3. Yapp and Poths (1995) were able to explain such D/H exchange data with a two-component model for the hydrogen in goethite (exchangeable HTN hydrogen and non-exchangeable structural hydrogen). The non-exchangeable hydrogen contains information on ancient environments of goethite crystallization. The following equations (Yapp and Poths, 1995) represent the hydrogen isotope atom balance in goethite after the D/H exchange experiments:

$$\delta D_t = m(1000 + \delta D_{fv}) + b \quad (3)$$

$$\delta D_s = \frac{\left[b + 1000\frac{m}{\alpha_{e-v}}\right]}{\left[1 - \frac{m}{\alpha_{e-v}}\right]} \quad (4)$$

$\delta D_t$ = the δD of the water recovered from the 850°C dehydration of goethite after exchange. $\delta D_{fv}$ = the δD of the vapor after exchange. $m$ and $b$ are the slope and intercept, respectively, of a straight line defined by the array of exchange data. $\delta D_s$ = the δD value of the nonexchangeable structural hydrogen in goethite. $\alpha_{e-v}$ is the hydrogen isotope fractionation factor between the exchangeable HTN hydrogen and the ambient water. Feng and Yapp (2008) determined a value for $\alpha_{e-v}$ of 0.942 for the types of exchange conditions represented by the results in Table 3.

Values of $\delta D_t$ from Table 3 are plotted against the corresponding values of $1000 + \delta D_{fv}$ in Fig. 5. As indicated by Eq. (3), any two pairs of accurate data would define a useful

Table 3
Data from hydrogen isotope exchange experiments on Ax-2.

| MHD # | Mass[a] (mg) | Exchange conditions | | | | After exchange | | | |
|---|---|---|---|---|---|---|---|---|---|
| | | Initial exchange $H_2O$ | | | 22 °C exchange time (min) | Goethite 850°C $H_2O$ | | Final exchange $H_2O$ | |
| | | Descriptor | μmol[b] | δD (‰) | | μmol | δD (‰) | μmol | δD (‰) |
| 2499 | 60.5 | DIW-1 | ~190 | +114 | 1080 | 265 | −122 | 204 | +36 |
| 2500 | 62.5 | EPNGW-6ct | ~220 | −252 | 1080 | 273 | −218 | 247 | −167 |
| 2533 | 58.9 | EPNGW-3ct | ~210 | −178 | 1080 | 271 | −209 | 226 | −148 |

[a] Initial mass of the Ax-2 aliquot.

[b] Estimated from the difference in weight between empty and filled (sealed) glass capillary tubes used to introduce the exchange water to the system. The uncertainty in the estimated amounts of initial exchange water is ~7% of the nominal value. The estimates tend to be low, because of an apparent negative drift of 0.2–0.3 mg in the nominal mass reported by the digital balance that was used to measure masses before and after loading and sealing the capillaries. The apparent underestimate of the initial amounts of exchange water did *not* affect the outcome or interpretation of these exchange experiments.

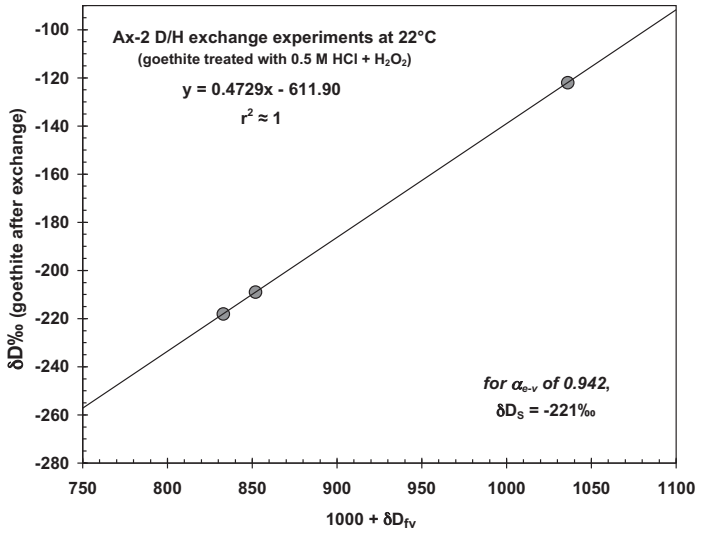


Fig. 5. Results of hydrogen isotope exchange experiments between Ax-2 goethite and water vapor at 22 °C. The slope and intercept of the linear regression of the data can be used to calculate a δD value ($\delta D_s$) of the non-exchangeable, structural hydrogen in the goethite. For this set of exchange experiments, with $\alpha_{e-v} = 0.942$, the $\delta D_s$ value of Ax-2 goethite is −221 (±6)‰. See text.

straight line in these types of experiments. There are three pairs of data (3 data points) in Fig. 5. The data point intermediate to the two extreme values in Fig. 5 plots on a regression line defined by those two extremes. This apparent linearity is consistent with the prediction of Eq. (3). The values of $m$ (0.4729) and $b$ (−611.90) from linear regression of the three data points in Fig. 5 and an $\alpha_{e-v}$ value of 0.942 in Eq. (4) yield a $\delta D_s$ value of −221 (±6)‰. More significant figures are shown for $m$ and $b$ than are justified by the analytical precision, but they were used in this form to minimize rounding errors in the calculation of $\delta D_s$. The $\delta D_s$ value of −221‰ is employed in subsequent discussion of the paleoenvironmental information recorded in the Ax-2 goethite.

### 3.3. Oxygen isotopes

#### 3.3.1. Relationship between measured yield and $\delta^{18}O$

Measured yields and $\delta^{18}O$ values of pre-treated aliquots of Ax-2 are listed in Table 4. The large amount of scatter in these data is an unexpected complication in the analysis of this material. Some of the Ax-2 oxygen yields are as low as 9.4 μmol/mg, which is well below the expected yield of 11.2 μmol/mg for stoichiometric FeOOH. The yields of 9.4 μmol/mg correspond to those expected for pure hematite, but the XRD results (Fig. 3) indicate that, in the powdered sample, goethite is the dominant mineral (with accessory hematite and minor lepidocrocite). Consequently, aliquots of pure hematite are not the source of the lowest

Table 4
Oxygen isotope analyses of aliquots of Ax-2.

| Lab # | Sample mass | | 22 °C $BrF_5$ pre-treatment | $O_2$ from 450 °C reaction | | Normalized $O_2$ yield[b] (μmol/mg) |
|---|---|---|---|---|---|---|
| | Initial (mg) | Adjusted[a] (mg) | Time (min.) | (μmol) | $\delta^{18}O$ (‰) | |
| 558 | 23.2 | 21.6 | 20 | 245 | −6.5 | 11.3 |
| 566 | 20.0 | 18.6 | 15 | 204 | −8.1 | 11.0 |
| 573 | 19.2 | 17.9 | 15 | 194 | −9.0 | 10.9 |
| 575 | 20.0 | 18.6 | 45 | 196 | −9.8 | 10.5 |
| 576 | 20.0 | 18.6 | 60 | 195 | −9.8 | 10.5 |
| 571 | 19.1 | 17.8 | 60 | 178 | −10.4 | 10.0 |
| 572 | 22.1 | 20.6 | 30 | 208 | −10.5 | 10.1 |
| 526 | 20.6 | 19.2 | 25 | 190 | −11.0 | 9.9 |
| 583 | 22.1 | 20.6 | 60 | 193 | −11.1 | 9.4 |
| 589 | 24.1 | 22.4 | 60 | 212 | −11.7 | 9.5 |
| F15787 | 9.6 | 8.9 | 60 | 84 | −11.8 | 9.4 |

[a] 7.0% of the initial open-to-air mass of Ax-2 is $H_2O$ that desorbs in vacuum at 100 °C. Vacuum outgassing at 22 °C plus subsequent 22 °C $BrF_5$ pre-treatment was presumed to remove most or all of the $H_2O$ that would otherwise have been removed if the sample had been outgassed at 100 °C (Yapp, 1987a,b). The mass of $H_2O$ corresponding to 7.0% of the initial sample mass was subtracted from that initial mass to obtain the adjusted mass of each aliquot of Ax-2.

[b] The normalized $O_2$ yield is with respect to the adjusted mass.

$O_2$ yields of Table 4. Conversely, the highest measured $O_2$ yield of 11.3 μmol/mg is higher than expected for a goethite sample that contains some admixed hematite.

In general, the lower oxygen yields in Table 4 are associated with longer $BrF_5$ pre-treatment times (e.g., 60 min). This is an unexpected result for such a comparatively pure goethite. For example, such low yields are not observed in pure synthetic goethite for room temperature pre-treatment times as long as 60 min (Yapp, 1987a). However, the Ax-2 data of Table 4 suggest that there may be an interpretable pattern, because lower, mass-normalized oxygen yields are systematically associated with more negative $\delta^{18}O$ values.

### 3.3.2. Pre-treatment model and the $\delta^{18}O$ value of Ax-2

The water desorbed from aliquots of Ax-2 by outgassing in vacuum at 22 °C, then 100 °C, represented an average of 7.0% of the initial, open-to-air, sample mass (Table 6). This large amount of adsorbed water, as well as the lowest $O_2$ yields, suggests a possible explanation for the results of Table 4. It was assumed that, with respect to the 22 °C $BrF_5$ pre-treatment, three relevant oxygen reservoirs characterize the Ax-2 goethite: (1) adsorbed molecular water ("*a*") which reacts with $BrF_5$ at 22 °C; (2) surface, goethite "hydroxyl" oxygen ("*sx*") that can react with $BrF_5$ at 22 °C; (3) the remainder of the oxygen in the goethite crystal structure ("*c*"), which does not react with $BrF_5$ at 22 °C on the time scales of these experiments. Published goethite infrared spectra are consistent with the presence of molecular water and surface hydroxyl (e.g., Boily et al., 2006).

At 22 °C, it was assumed that $BrF_5$ reacts with adsorbed molecular water (*a*) at a faster rate than with surface hydroxyl oxygen (*sx*). Also, because $BrF_5$ is present in excess, these 22 °C reaction rates were presumed to be pseudo-first order in the amount of oxygen in the reservoir of interest (e.g., $dn_a/dt = -k_a n_a$; where, $k_a$ = the rate constant for reaction of $BrF_5$ with reservoir $a$ ; $n_a$ = moles of oxygen

Table 5
IAEA/WMO precipitation and temperature data from Ellesmere Island, Canada.

| Ellesmere Island | Average modern precipitation | | *T* (°C) |
|---|---|---|---|
| | $\delta D$ (‰)$_{SMOW}$ Annual | $\delta^{18}O$ (‰)$_{SMOW}$ Annual | Annual |
| Alert | −217 | −27.7 | −17.9 |
| Eureka | −205 | −25.5 | −19.4 |
| | Summer (J-J-A) | Summer (J-J-A) | Summer |
| Alert | −175 | −23.3 | 1.4 |
| Eureka | −165 | −20.6 | 4.0 |

As reported by the IAEA, Alert is located at latitude 82.3°N and longitude 62.2°W, and Eureka is located at latitude 80.0°N and longitude 85.56°W. Average values of $\delta D$ and $\delta^{18}O$ are precipitation amount-weighted averages.

Table 6
Data from incremental dehydration-decarbonation of Ax-2 aliquots.

| MHD # | Fraction | Time (min) | *T* (°C) | $H_2$ (μmol) | $CO_2$ | | $X_v(H_2)$ | *F* |
|---|---|---|---|---|---|---|---|---|
| | | | | | μmol | $\delta^{13}C$ | | |
| *MHD-2066 initial sample mass = 257.9 mg* | | | | | | | | |
| 2066 | 1 | 55 | 22 and 100 | 928 | 6.0 | 1.8 | — | 0.0065 |
| 2066 | 2 | 30[a] | 215[a] | 686 | 54.5 | −5.5 | 0.49 | 0.079 |
| 2066 | 3 | 30 | 215 | 462 | ***11.6*** | ***6.8*** | 0.83 | ***0.025*** |
| 2066 | 4 | 30 | 215 | 28 | 0.9 | 2.1 | 0.85 | 0.032 |
| 2066 | 5 | 60 | 215 | 23 | 0.7 | −0.6 | 0.86 | 0.030 |
| 2066 | 6 | 30[a] | 850[a] | 192 | 29.5 | 4.5 | 1.00 | 0.154 |
| *MHD-2331 initial sample mass = 206.1 mg* | | | | | | | | |
| 2331 | 1 | 111 | 23 and 100 | 845 | 6.2 | 3.8 | — | 0.0073 |
| 2331 | 2 | 30[a] | 180[a] | 204 | 33.0 | −6.7 | 0.23 | 0.162 |
| 2331 | 3 | 21 | 155–175 | 199 | 3.2 | −1.7 | 0.44 | 0.016 |
| 2331 | 4 | 30 | 173 | 261 | ***5.8*** | ***6.5*** | 0.73 | ***0.022*** |
| 2331 | 5 | 30 | 173 | 43 | ***1.3*** | ***5.8*** | 0.78 | ***0.030*** |
| 2331 | 6 | 60 | 173 | 22 | 0.7 | 1.2 | 0.80 | 0.032 |
| 2331 | 7 | 120 | 173 | 16 | 0.7 | −1.9 | 0.82 | 0.044 |
| 2331 | 8 | 31[a] | 850[a] | 161 | 23.0 | 1.9 | 1.00 | 0.143 |

$X_v(H_2)$ is the cumulative evolved hydrogen as a mole fraction of the total hydrogen in the sample. $X_v(H_2)$ is calculated exclusive of the hydrogen in water outgassed at 22 and 100 °C. $F = nCO_2/nH_2O$. Where, $nCO_2$ = μmol of $CO_2$ evolved in a single dehydration step, and $nH_2O$ = μmol of water recovered in that step. Values in bold italics indicate $CO_2$ from the $Fe(CO_3)OH$ component.

[a] Closed system in ~0.16 bar pure $O_2$. All other increments open system dehydration in vacuum (e.g., Yapp and Poths, 1991, 1993; Hsieh and Yapp, 1999).

in $a$; $t$ = time; and so forth for $sx$ and $c$). Finally, it was assumed that there is no oxygen isotope fractionation associated with each of the respective reactions at 22 °C. These assumptions yield the following atom balance equations:

$$\delta^{18}O = \frac{\delta^{18}O_a\left(\frac{n_{a_0}}{M}\right)e^{-t/\tau_a} + \delta^{18}O_{sx}\left(\frac{n_{sx_0}}{M}\right)e^{-t/\tau_{sx}} + \delta^{18}O_c\left(\frac{n_{c_0}}{M}\right)e^{-t/\tau_c}}{[O_2]} \quad (5a)$$

$$[O_2] = \left(\frac{N}{M}\right) = \left\{\left(\frac{n_{a_0}}{M}\right)e^{-t/\tau_a} + \left(\frac{n_{sx_0}}{M}\right)e^{-t/\tau_{sx}} + \left(\frac{n_{c_0}}{M}\right)e^{-t/\tau_c}\right\} \quad (5b)$$

$\delta^{18}O$ = the $\delta^{18}O$ value measured for the Ax-2 sample that remains after the 22 °C pre-treatment, and $N$ = the measured moles of $O_2$ in that sample. $M$ = the mass of the mineral sample adjusted for removal of adsorbed water (see footnote to Table 4). $[O_2]$ as defined in Eq. (5b) is the mass-normalized oxygen yield (μmol/mg). $\tau_a$, $\tau_{sx}$ and $\tau_c$ ($\tau = 1/k$) are characteristic times for reaction of the indicated oxygen reservoir with $BrF_5$ at 22 °C. $\tau_c \to \infty$, for reservoir $c$, because it is assumed that $c$ does not react with $BrF_5$ at 22°C. $n_{a_0}$, $n_{sx_0}$, and $n_{c_0}$ are the initial moles of oxygen in reservoirs $a$, $sx$, and $c$, respectively. $\delta^{18}O_a$, $\delta^{18}O_{sx}$ and $\delta^{18}O_c$ are, respectively, the $\delta^{18}O$ values (presumed to be constant) of oxygen reservoirs $a$, $sx$, and $c$. Assignment of values for the various $n_{i_0}/M$ and $\delta^{18}O_i$ terms, specification of the ratio $\tau_{sx}/\tau_a$, and use of increments of dimensionless time ($t/\tau_{sx}$) permit straightforward calculation of paired values for $\delta^{18}O$ and $[O_2]$ using parametric Eqs. (5a) and (5b).

As an example, the following model input values were used: $(n_{a_0}/M) = 1.25$ μmol/mg; $(n_{sx_0}/M) = 1.25$ μmol/mg; $(n_{c_0}/M) = 9.45$ μmol/mg; $\delta^{18}O_a = 47.2‰$; $\delta^{18}O_{sx} = 4.5‰$; and $\delta^{18}O_c = -11.5‰$. A non-zero value for $(n_{a_0}/M)$ implies that some adsorbed water remained on a sample after outgassing in vacuum at 22 °C (e.g., Boily et al., 2006). These input values were intended to be heuristic and were chosen to aid the interpretation of measured results in Table 4. Calculated model values of $\delta^{18}O$ and $1/[O_2]$ are plotted in Fig. 6a. The different reaction-trajectory curves of Fig. 6a correspond to different choices of "$\beta$", where $\beta = \tau_{sx}/\tau_a$. Increasing values of $\beta$ imply increasingly faster rates of reaction with adsorbed water ($a$) relative to surface hydroxyl oxygen ($sx$).

For the input parameters used in the calculation, the curves in Fig. 6a show that the predicted value of $\delta^{18}O$ should decrease as $1/[O_2]$ increases (i.e., $[O_2]$ decreases). For $\beta = 1$, the model yields a straight line mimicking two-component mixing. For increasing values of $\beta$, the modeled relationship becomes increasingly curvilinear until at very large departures of $\beta$ from unity (e.g., $\beta = 100$), the predicted relationship between $\delta^{18}O$ and $1/[O_2]$ approximates two straight-line segments (A and B in Fig. 6a) with distinctly different slopes. A value for $\beta$ of 100 implies that the reaction of $BrF_5$ with adsorbed water at 22 °C is so rapid (segment A, in Fig. 6a) that it is essentially complete before there is any significant loss of oxygen from the reaction between $BrF_5$ and $sx$ (segment B).

Extrapolations of linear regressions (thick, solid lines in Fig. 6a) of the extremum portions of segments A and B intersect at $[O_2] = 10.7$ μmol/mg and $\delta^{18}O = -9.7‰$. These values correspond to the model input values of $[O_2] = 10.7$ μmol/mg and $\delta^{18}O = -9.7$ ‰ (derived from combination of the input values for the $sx$ and $c$ reservoirs), but such close correspondence is only achieved when this regression method is applied to model curves for which $\beta$ is a large value.

To explore another possibility, a modified version of this model was developed that incorporated Rayleigh-type fractionation in each of the reactions with $BrF_5$ at 22 °C. At high values of $\beta$, two distinct nonlinear segments of the reaction trajectory were present, but their mutual "intersection" (i.e., abrupt change in slope) corresponded, as it must for large $\beta$ values, to the oxygen yield and $\delta^{18}O$ value of the model goethite. Therefore, since the key feature is the abrupt change in slope, the simpler non-Rayleigh model represented by Eq. (5) provided the rationale for determination of the oxygen yield and $\delta^{18}O$ value of the goethite in Ax-2.

For Ax-2 (after pre-treatment with $BrF_5$ at 22 °C), measured $\delta^{18}O$ values are plotted against corresponding values of $1/[O_2]$ in Fig. 6b. The data array in Fig. 6b is similar to the model results of Fig. 6a for $\beta = 100$. The three data points (gray circles) in Fig. 6b that represent smaller amounts of oxygen removed by pre-treatment appear to define a steeply sloping linear array. On the other hand, the data points (black triangles) from aliquots with higher degrees of oxygen removal define an apparently different linear array with a shallower slope. Therefore, separate linear regressions of these two groups of data were used to determine the "structural" values of $[O_2]$ and $\delta^{18}O$ in Ax-2 (i.e., the sample values after adsorbed water has been removed, but before removal of surface hydroxyl oxygen). The lines and equations in Fig. 6b represent the respective regressions.

The intersection of the line segments of Fig. 6b corresponds to $[O_2] = 10.7$ μmol/mg. This value represents 96% of the yield expected for pure FeOOH. As discussed previously, there is some accessory hematite and minor lepidocrocite in Ax-2. Lepidocrocite (γ-FeOOH) would have no effect on the expected oxygen yield, but the presence of hematite in the sample mixture should produce yields somewhat less than the 100% expected for pure goethite, and a yield of 96% is consistent with this expectation. This result lends credence to the idea that the intersection of the two line segments in Fig. 6b provides information on the amount of structural oxygen in Ax-2.

Application of the $[O_2]$ value of 10.7 μmol/mg to each of the regression equations of Fig. 6b yields $\delta^{18}O$ values of $-9.6‰$ and $-9.7‰$. These two $\delta^{18}O$ values differ because of rounding in the regression equations and in the value of $[O_2]$. The apparent difference is less than the analytical uncertainty, and a goethite $\delta^{18}O$ value of $-9.6‰$ is used in subsequent discussion.

The greatest uncertainty in the regressions of Fig. 6b arises from use of adjusted masses to determine the individual values of $[O_2]$ in Table 4. As a test of the robustness of the line segment approach used here, $[O_2]$ values for individual aliquots of Ax-2 were determined using the initial sample masses in Table 4. Linear regressions of the measured $\delta^{18}O$ values against unadjusted values of $1/[O_2]$ yielded, for the

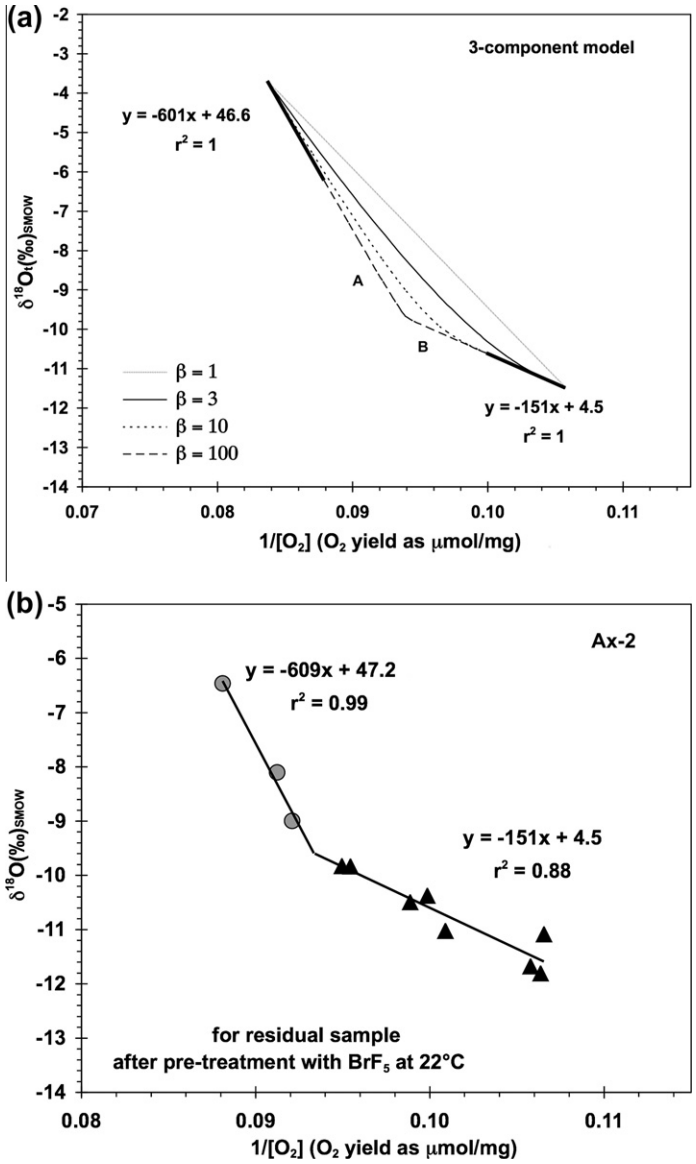


Fig. 6. (a) Model curves for the relationship between the $\delta^{18}O$ of residual oxygen and the reciprocal of the concentration of the residual oxygen in goethite after pre-treatment with $BrF_5$ at 22 °C. The labels "A" and "B" identify the two apparently linear line segments (dashed lines) for the model result with $\beta = 100$. The thick, solid line segments represent linear regressions of the extremum values of line segments A and B. The corresponding regression equations are shown on the figure. See text. (b) Measured $\delta^{18}O$ values of residual Ax-2 oxygen plotted against the reciprocal of the measured residual oxygen concentration for aliquots of Ax-2 after pre-treatment with $BrF_5$ at room temperature. The two solid lines in (b) represent the respective linear regressions of the two subsets of measured data (gray circles and black triangles) with the corresponding regression equations. See text.

early portion of the process, $\delta^{18}O = -769\ (1/[O_2]) + 63.5$, with $r^2 = 0.98$; and for the later, lower yield portion, $\delta^{18}O = -119\ (1/[O_2]) + 1.7$, with $r^2 = 0.89$. The slopes and intercepts of these alternative regression lines are different from those in Fig. 6b, but they yield calculated values of $[O_2]$ and $\delta^{18}O$ for structural oxygen in Ax-2 of 10.5 μmol/mg and −9.6‰, respectively. These values are analytically indistinguishable from those determined from Fig. 6b. This apparent robustness may be a consequence of the proximity of some the data points to the intersection of the regression lines, thus constraining the inferred Ax-2 values.

Therefore, the following values are adopted for Ax-2: $[O_2] = 10.7\ (\pm 0.4)$ μmol/mg and $\delta^{18}O = -9.6\ (\pm 0.5)$‰. The estimated uncertainties are larger than desirable, but at present there are no alternative methods of acquiring the information from this material.

### 3.4. Implications of D/H and $^{18}O/^{16}O$ in Ax-2

#### *3.4.1. Paleotemperature and ancient waters*

Several studies have shown that the δD and $\delta^{18}O$ values of goethite reflect the waters present at the time of

crystallization and have successfully combined goethite δD and $\delta^{18}O$ data to characterize modern and ancient climate conditions (e.g., Yapp, 1987a, 1993, 1997, 1998, 2000, 2008; Girard et al., 2000; Tabor et al., 2004a; Tabor and Yapp, 2005; Hren et al., 2006).

The δD (−221‰) and $\delta^{18}O$ (−9.6‰) values of goethite-dominated Ax-2 indicate crystallization in the presence of meteoric water. The temperature of crystallization of the mineral can be determined if the δD and $\delta^{18}O$ values of that ancient meteoric water corresponded closely to the modern global meteoric water line (GMWL) of Craig (1961), where the GMWL is $\delta D = 8\delta^{18}O + 10$. The relevant equation is adapted from Savin and Epstein (1970):

$$\delta D_G = 8\left(\frac{^{D}\alpha_G}{^{18}\alpha_G}\right)\delta^{18}O_G + 1000\left[8\left(\frac{^{D}\alpha_G}{^{18}\alpha_G}\right) - 1\right] - 6990\,^{D}\alpha_G \quad (6)$$

$\delta D_G$ and $\delta^{18}O_G$ are the measured δD and $\delta^{18}O$ values of FeOOH. $^{D}\alpha_G$ and $^{18}\alpha_G$ are hydrogen and oxygen isotope fractionation factors, respectively, between FeOOH and liquid water. $^{18}\alpha_G$ is temperature dependent and values of $^{D}\alpha_G$ and $^{18}\alpha_G$ for this work were taken from Yapp (1987a,b, 2007) for reasons which are discussed in Yapp (2000, 2001a, 2007).

There is presently no independent confirmation of the presence of GMWL-type waters on Axel Heiberg Island at the time of Ax-2 goethite crystallization. However, precipitation-weighted average annual and average summer (J-J-A) isotopic compositions of recent precipitation at Eureka and Alert (Table 5) on nearby Ellesmere Island (Fig. 1) correspond well to the GMWL (Fig. 7a). As a working hypothesis, it is assumed that average ancient precipitation on Axel Heiberg Island was also GMWL-type water.

Goethite isotherms (dashed lines) calculated with Eq. (6) are shown in Fig. 7b together with the measured δD and $\delta^{18}O$ values of Ax-2 (filled circle). Also plotted in Fig. 7b is a hypothetical, modern summer goethite (filled triangle) calculated from the averages of the summer (J-J-A) temperatures and isotopic compositions of precipitation on Ellesmere Island (Table 5). Miscellaneous published goethite data (gray squares) are included in Fig. 7b to provide context.

The presence of some hematite and minor lepidocrocite in Ax-2 might complicate a simple interpretation of the oxygen and hydrogen isotope data. However, the results of low-pH synthesis experiments (Yapp, 1990) and studies of natural samples (e.g., Girard et al., 2002; Tabor, 2007) indicate that goethite and hematite may exhibit the same, or very similar, mineral-water oxygen isotope fractionations over a range of sedimentary and early diagenetic temperatures. Lepidocrocite-water fractionation factors are not known, but the fact that it is a polymorph of FeOOH suggests that the mineral-water isotopic fractionation factors for lepidocrocite are similar to goethite. Moreover, lepidocrocite is only a minor mineral in Ax-2 (Fig. 3) and thus would be a small contributor to the isotopic composition of the sample.

From Fig. 7b, the temperature of crystallization of Ax-2 is 3 (±5)°C. This inferred temperature of crystallization (~3 °C) is among the coldest determined thus far for a natural goethite. The goethite temperature of 3 °C contrasts with the modern MAT (mean annual surface air temperature) of approximately −19 °C on nearby Ellesmere Island (Table 5), but it is comparable to the modern average summer (J-J-A) temperature of about 3 °C. Although this could indicate that the hydrogen and oxygen isotopes in Ax-2 record conditions essentially the same as local, modern summers, upon closer examination, such a conclusion is not supported.

The measured Ax-2 data, together with $^{D}\alpha_G$ and $^{18}\alpha_G$, were used to calculate a δD value of −139 (± 6)‰ and $\delta^{18}O$ value of −18.6 (±0.8)‰ for the liquid water present at the time of goethite crystallization. These ancient water values contrast significantly with the two-site, average δD and $\delta^{18}O$ values of about −170‰ and −22.0‰, respectively, for modern summer precipitation on Ellesmere Island (Table 5). This contrast is clearly illustrated by the difference between the measured Ax-2 goethite data and the hypothetical modern summer goethite in Fig. 7b. However, before discussing the paleoenvironmental implications of these results, it is useful to consider the additional constraint that they provide on the minimum age of crystallization of Ax-2 goethite.

### 3.4.2. Possible H and O isotope constraint on minimum sample age

The more positive δD and $\delta^{18}O$ values of meteoric water recorded by Ax-2 reflect ancient environmental conditions different from modern. Isotope measurements of the Greenland and Antarctic ice sheets show that for much of the Pleistocene the δD and $\delta^{18}O$ values of high latitude meteoric waters were similar (interglacial) to, or more negative (glacial) than, modern values (e.g., Johnsen et al., 2001; Lambert et al., 2008). This observation leads to a conclusion that the sampled mass of the Ax-2 goethite pre-dates the Pleistocene, which is consistent with the late Miocene to Pliocene nominal ages of ~5.5–2.8 Ma obtained from the (U–Th)/He data for 4 of the 6 aliquots of Table 1.

If the age of crystallization of Ax-2 goethite is actually ~5.5–2.8 Ma, the two nominal Pleistocene ages in Table 1 (0.6 and 0.9 Ma) require some additional consideration. Spuriously young (U–Th)/He ages might arise in small volumes of Ax-2 for which one or more of the following conditions existed: (1) presence of extremely small goethite crystals (higher degrees of diffusive He loss); (2) locally high porosity and permeability (loss of $^{4}He$ by α-ejection); and/or (3) relatively recent, localized, reductive dissolution of small amounts of goethite and removal of some of the $Fe^{2+}$ product with retention of the relatively insoluble Th and adsorption of the U on the remaining goethite (e.g., Langmuir, 1978; Rai et al., 2000; Neck et al., 2003; Sherman et al., 2008).

With respect to conditions 2 and 3, there is some evidence for localized, relatively large pores (~10 μm) in Ax-2 (contrast the comparatively non-porous area of Ax-2 in Fig. 8a with the porous area in Fig. 8b). Also, the presence of minor lepidocrocite in Ax-2 (Fig. 3) is consistent with some oxidation-reduction ("redox") cycling of Fe (e.g., Schwertmann, 1988). Moreover, condition 3 would result in locally high concentrations of U and Th as well as

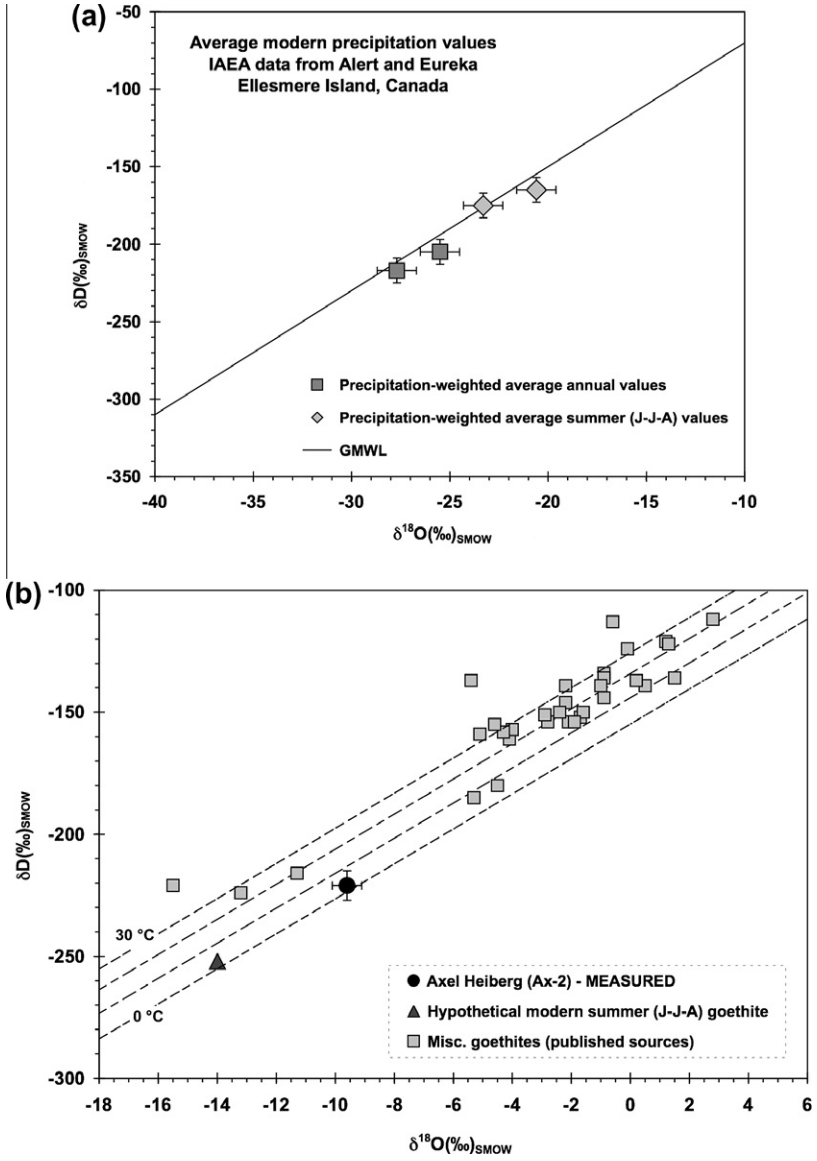


Fig. 7. (a) Precipitation amount-weighted δD plotted against $\delta^{18}O$ for average annual and average summer (J-J-A) values of modern precipitation at two sites (Alert and Eureka) on Ellesmere Island in the Canadian Arctic as measured by the IAEA/WMO (2004). The solid line is the GMWL of Craig (1961). Note that the averages of the measured values correspond closely to the GMWL. See text. (b) Measured value of δD plotted against $\delta^{18}O$ for Ax-2 goethite (black circle). The gray squares represent published values for goethites from various locales and are included as a basis for comparison (Girard et al., 2000; Yapp, 2000). The black triangle represents a hypothetical goethite crystallized from average modern summer precipitation at average modern summer (J-J-A) temperatures (see Table 5). Dashed lines are isotherms for goethite crystallized in the presence of GMWL-type precipitation. The plotted isotherms represent increments of 10 °C over the range from 0 to 30 °C. The temperature of crystallization of Ax-2 goethite indicated by the result in (b) is 3 (±5)°C. Note the contrast between the measured δD and $\delta^{18}O$ values of Pliocene Ax-2 goethite and the values for a hypothetical modern goethite formed in the summer (J-J-A) even though the ancient and modern temperatures are comparable (see text).

nominally younger ages for the hypothesized volumes hosting such activity. It is noteworthy that the micro-aliquots with the two youngest nominal ages (0.6 and 0.9 Ma) have the highest measured U and Th concentrations in Table 1.

In the absence of significant re-precipitation of goethite (and/or lepidocrocite) within Ax-2, minor condition 3-type dissolution of a small fraction of the original goethite would not be expected to have an important effect on the H, C, and O isotope compositions of the total residual Ax-2. Thus, the measured stable isotope composition of Ax-2 is presumed to preserve information on a latest Miocene to Pliocene environment of goethite crystallization (four oldest ages of Table 1).

### 3.4.3. Arctic seasonality and Ax-2

Elias and Matthews (2002) used fossil beetle assemblages to estimate surface air temperatures in the Canadian Arctic during the Pliocene on two islands adjacent to, and bracketing, Axel Heiberg Island (Meighen Island to the west and Ellesmere Island to the east). Their results suggest

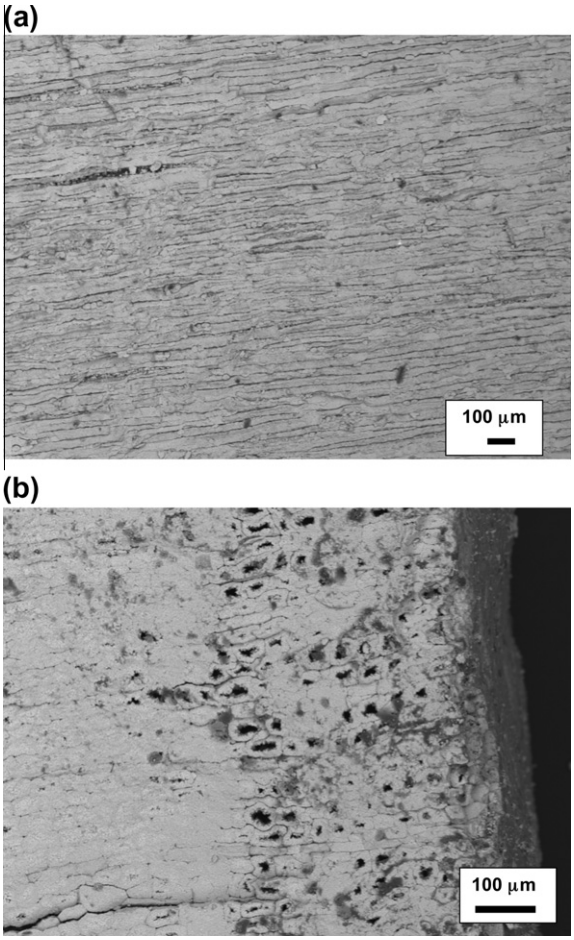


Fig. 8. (a) SEM image of a relatively non-porous region of Ax-2. (b) SEM image of a relatively porous portion of Ax-2. See text for discussion.

that Pliocene (~3–3.5 Ma) maximum summer temperatures at the two sites were about 12 (±2)°C and that minimum winter temperatures might have been −25 (±2)°C. If the variation of seasonal temperature was sinusoidal (as it is at present), these Pliocene seasonal extremes indicate an average annual temperature in that region of −7 to −6 (± 4)°C. This compares with a mean annual temperature (MAT) of −6 (±2)°C estimated from the oxygen isotope composition of well-preserved Pliocene (~4 Ma) trees on Ellesmere Island (Ballantyne et al., 2006). However, Ballantyne et al. (2010a) published revised estimates of the Pliocene (~4 Ma) MAT on Ellesmere Island based on a new estimate of the $\delta^{18}O$ value of the ancient ambient water and using three proxies: (1) tree ring oxygen isotopes and ring widths, $T = -0.5 \pm 1.9$ °C; (2) coexistence of ancient vegetation, $T = -0.4 \pm 4.1$ °C; and (3) paleosol bacterial tetraether, $T = -0.6 \pm 5.0$ °C). A Pliocene MAT of −0.4 °C is much warmer than the modern MAT of about −20 to −18 °C on either Axel Heiberg or Ellesmere Island (Table 5; also Jahren, 2007, and references therein). In addition, Ballantyne et al. (2010a) estimated a Pliocene cold month mean temperature of about −12 °C and a warm month mean temperature of about 14 °C, which indicates a smaller degree of thermal seasonality than at present.

Goethite precipitates from liquid water (e.g., Schwertmann, 1988). Thus, for freshwater environments, the presence of goethite implies temperatures of crystallization ⩾0 °C, which is consistent with the value of 3 (±5)°C inferred for Ax-2. The contrast between the temperature of about 3 °C calculated from the isotopic composition of Ax-2 goethite and the MAT of −6 °C (Elias and Matthews, 2002) or −0.4 °C (Ballantyne et al., 2010a) deduced from biological proxies might have its origins in differences in the specific local environments recorded by the different proxies. Moreover, the different temperatures might also reflect the fact that the different proxies were not precisely contemporaneous in the Pliocene and recorded environmental information on different time scales (e.g., up to millions of years for formation of Ax-2 goethite and up to decades for the life cycles of the biological proxies). The question of possible differences in local environments of formation is addressed here.

Ancient plants (trees, etc.,) grew at the lithosphere-atmosphere interface and would have experienced surface conditions directly. Ax-2 goethite, on the other hand, formed in the subsurface when the environment within parts of the Buchanan Lake Formation became oxidizing, possibly subsequent to uplift in the waning stages of the Tertiary Eurekan orogeny (e.g., Harrison et al., 1999).

Seasonal variations of temperature are increasingly attenuated with increasing depth below Earth's solid surface (e.g., Jury et al., 1991), until at depths of a few meters the subsurface temperature is nearly constant at the average annual surface value. In this context, it seems that the seasonality of Pliocene Arctic surface air temperatures, although smaller than modern, was still substantial (Elias and Matthews, 2002, an annual range of ~37 °C; or Ballantyne et al., 2010a, an annual range of ~26 °C). If the Pliocene Arctic MAT at the time of formation of Ax-2 goethite was either −6 or −0.4 °C, the goethite would not be expected to have crystallized at depths greater than a few meters, because water at these somewhat greater depths would presumably have been frozen year round. Crystallization at shallower depths would imply that Ax-2 goethite preserved a seasonally selective temperature representing some average over an interval of time when the ambient subsurface temperatures were ⩾0 °C. These possible depths of crystallization can be constrained to some extent by consideration of a simple conductive heat flow model.

Carslaw and Jaeger (1959) and Jury et al. (1991) discuss the conductive heat flow equation for a semi-infinite solid (local solid Earth) with sinusoidally varying temperature as the upper boundary condition (i.e., surface air temperature):

$$T(z,t) = T_{\mathrm{MAT}} + Ae^{-\left(\frac{z}{L}\right)} \sin\left(\frac{2\pi}{\tau}t - \frac{z}{L}\right) \quad (7)$$

$t$ = time. $\tau$ = the period of the sinusoidal variation (12 months for seasonal variation of surface air temperature). $z$ = depth below the surface (positive and increasing with increasing depth). $L$ = the characteristic depth, which is related to the thermal diffusivity (e.g., Jury et al., 1991). $T_{\mathrm{MAT}}$ = the mean annual surface air temperature (in °C). $A$ = the amplitude (in °C) of the seasonal variation of

surface air temperature. $T(z, t)$ = the temperature at some $z$ and $t$ in the subsurface.

For the current work, Eq. (7) was integrated to calculate average temperatures at various depths below the surface over intervals of time for which the temperatures at those depths were above 0 °C (i.e., liquid water).

$$\bar{T}_z^* = \frac{\int_{t_1}^{t_2} T(z,t)\mathrm{d}t}{\int_{t_1}^{t_2} \mathrm{d}t} \tag{8a}$$

$$\bar{T}_z^* = T_{\mathrm{MAT}} - \frac{A\tau}{2\pi}\frac{\left[\cos\left(\frac{2\pi}{\tau}t_2 - \frac{z}{L}\right) - \cos\left(\frac{2\pi}{\tau}t_1 - \frac{z}{L}\right)\right]}{t_2 - t_1} e^{-\left(\frac{z}{L}\right)} \tag{8b}$$

$\bar{T}_z^*$ = the average temperature at some depth $z$ over the time interval for which the ambient temperature at that depth is >0 °C. $t_1$ = the time at which the subsurface temperature at some depth $z$ rises above 0 °C, whereas $t_2$ is the moment when the ambient temperature at that depth drops below 0 °C. In other words, the interval from $t_1$ to $t_2$ corresponds to the relatively warm thermal pulse from "summer" surface air temperatures. All other terms are as defined for Eq. (7). The values of $t_1$ and $t_2$ at various depths and for specified values of $T_{\mathrm{MAT}}$, $A$, and $L$ were determined from Eq. (7). Using the results of Ballantyne et al. (2010a) as an approximate guide, the values chosen for model calculations were $T_{\mathrm{MAT}} = -0.4$ °C and $A = 13$ °C. From Elias and Matthews (2002), $T_{\mathrm{MAT}} = -6$ °C and $A = 18$ °C. Two values were used for $L$ (200 and 338 cm) as calculated from two extreme values for the thermal diffusivity of wet sand tabulated in Jury et al. (1991).

Calculated values of $\bar{T}_z^*$ are plotted against $z$ in Fig. 9. Paired curves for a particular surface air MAT in Fig. 9 represent the two values chosen for $L$. The results in Fig. 9 indicate that for an Ax-2 temperature of ~3 °C, which is presumed to correspond to $\bar{T}_z^*$, the depth of crystallization might have been, depending upon choice of MAT and amplitude, between about 100 and 450 cm at the time of crystallization. As seen in Fig.9, the greater depths of crystallization are associated with the higher model MAT of −0.4 °C. The applicability of the curves to crystallization of goethite is limited by the limitations of the model assumptions. For instance, surface temperature of the soil rather than air temperature may be a somewhat better choice for the upper boundary condition, and simple conduction of heat may be perturbed by advective heat transport by infiltrating rain or melt water (e.g., Jury et al., 1991). Also, the date at which the temperature drops below 0 °C at various depths lags behind the date at which that happens at the surface (e.g., by about 2 weeks at $z = 100$–200 cm). If surface freezing restricted the transport of oxygen to the subsurface, it would prematurely terminate the oxidation process (i.e., the formation of goethite). Therefore, the average predicted temperature of goethite formation at each depth would be slightly warmer than indicated by the curves of Fig. 9.

Nevertheless, for regions with high degrees of seasonality in surface air temperatures, the curves of Fig. 9 illustrate the important role that depth of formation could play in determining the temperatures preserved by minerals crystallized in the subsurface, especially when MAT <0 °C. From Eqs. (7) and (8) and Fig. 9, the temperature of ~3 °C (for Ax-2) at depths of 100–200 cm (MAT ≈−6 °C) would represent crystallization over the months from about June into September, whereas at a depth of ~450 cm for surface MAT ≈−0.4 °C, crystallization might have occurred over the months from July to December in the late Miocene/Pliocene Arctic climate. It should be noted that Ax-2 was collected from an outcrop of a paleosol. We have no independent information on its actual depth below the surface at the time of crystallization in the late Miocene/Pliocene.

### 3.4.4. Comparison with other Tertiary isotopic proxies on Axel Heiberg and Ellesmere

There are very few determinations of the $\delta^{18}O$ values of Tertiary meteoric waters on Axel Heiberg or Ellesmere

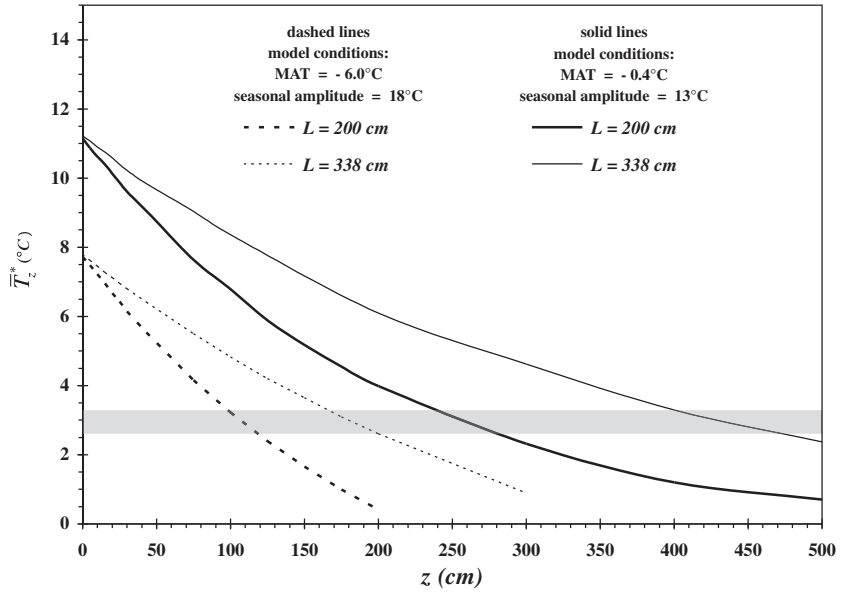


Fig. 9. Model curves for the average subsurface temperature, $\bar{T}_z^*$, at some depth ($z$) over the time intervals for which the temperatures at each depth of interest exceed 0 °C. The two curves represent results calculated for characteristic depths ($L$) of 200 and 338 cm (see text).

Islands. However, comparison of published results with those of Ax-2 might provide insight into possible seasonal bias in the isotopic data from surface or near-surface Arctic proxies. The $\delta^{18}O$ value of $-18.6$ ($\pm 0.8$)‰ determined herein for late Miocene/Pliocene meteoric water on Axel Heiberg Island is more positive than the Pliocene ($\sim$4 Ma) value of $-23.5$ ($\pm\sim 2$)‰ originally reported by Ballantyne et al. (2006) for Ellesmere Island, but comparable to the revised Ballantyne et al. (2010a,b) estimate of $-16.4$ ($\pm 1$)‰ (Fig. 10a).

Earlier in the Tertiary (middle Eocene $\sim$45 Ma), $\delta^{18}O$ values of meteoric waters that passed through trees during the growing season on Axel Heiberg Island appear to have ranged from about $-20$‰ to $-12$‰ (Jahren and Sternberg, 2003, 2008) with an average value of $-16$ ($\pm\sim 2$)‰ (Fig. 10a). Eberle et al. (2010) measured $\delta^{18}O$ values of phosphate in early Eocene ($\sim$52 Ma) fossil teeth and bones from a mammal and fish, respectively, on Ellesmere Island to deduce a $\delta^{18}O$ value for river water of about $-20.3$ ($\pm 1.4$)‰, which they interpreted as an average annual value. They also analyzed the phosphate in fossil turtle bone and estimated a $\delta^{18}O$ value of about $-17.5$ ($\pm 0.6$)‰ for the river water in the summer months of the early Eocene (Fig. 10a).

At present, the summer precipitation (J-J-A) on Ellesmere Island is about 37% of the total annual precipitation at Alert and about 53% at Eureka (IAEA/WMO, 2004). Therefore, average summer precipitation for the two sites taken together constitutes about 45% of the total annual precipitation. The large proportion of the annual total contributed by the summer precipitation (with its higher $^{18}O$ content) seems to account for the comparatively small difference of $\sim$4.5‰ between the average $\delta^{18}O$ values of modern, amount-weighted, summer and annual precipitation (Fig. 10a, Table 5). If a similar, or even more pronounced, summer weighting existed in the early Eocene Arctic, it might explain much of the small difference of about 3‰ between the $\delta^{18}O$ values for annual and summer river water on Ellesmere Island discussed by Eberle et al. (2010).

With the exception of the superseded results of Ballantyne et al. (2006), all of the nominal $\delta^{18}O$ values of ancient water in Fig. 10a are more positive than the modern summer value. These positive shifts in the inferred $\delta^{18}O$ values

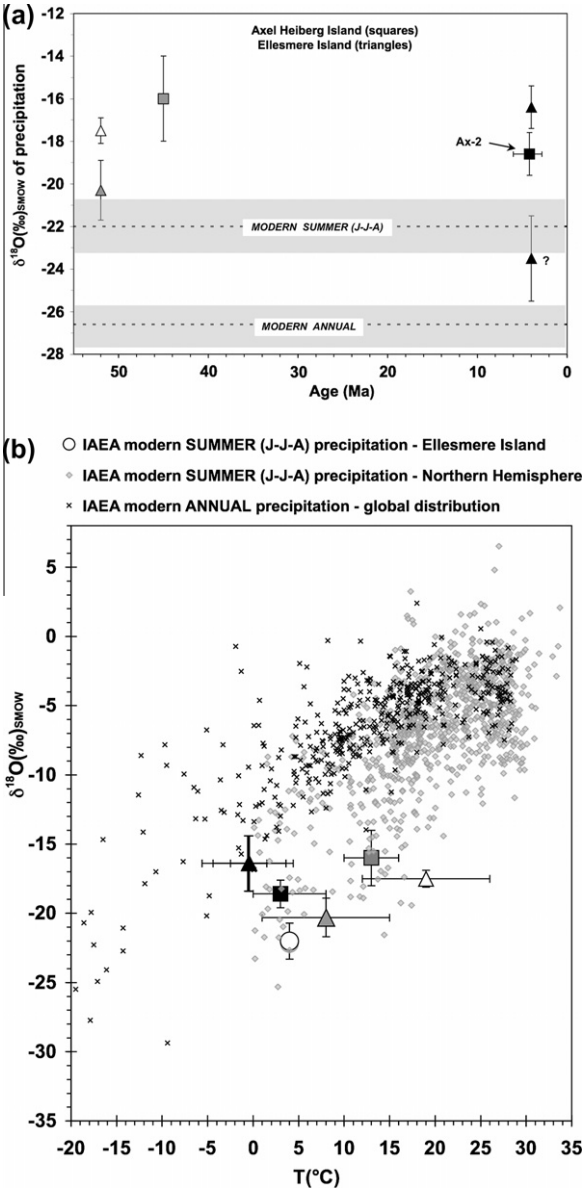


Fig. 10. (a) Plot of the inferred $\delta^{18}O$ values of ancient waters present at the indicated times of formation of various Eocene (gray and white squares and triangles) or Pliocene (black square and black triangle) isotopic proxies on Axel Heiberg (squares) and Ellesmere (triangles) Islands. Also shown for reference, are the two-site, amount weighted, average $\delta^{18}O$ values of modern summer (J-J-A) and annual precipitation (horizontal gray bands centered on dashed horizontal lines) as reported by the IAEA/WMO (2004) for the Alert and Eureka sites on Ellesmere Island. The question mark next to one black triangle refers to results from Ballantyne et al. (2006). See text. (b) $\delta^{18}O$ values of precipitation plotted against corresponding temperatures. Data from Eocene proxies are represented by gray and white squares and triangles, and data from Pliocene proxies by a black square and black triangles. All triangular symbols (irrespective of shading) are data from proxies on Ellesmere Island, whereas the square symbols (irrespective of shading) are data from proxies on Axel Heiberg Island. Black square: late Miocene/Pliocene data from this work. Gray square: middle Eocene data from Jahren and Sternberg (2003, 2008). Black triangle: Pliocene data from Ballantyne et al. (2010a,b). Gray and white triangles: early Eocene data from Eberle et al. (2010); the white triangle is their estimate of summer river water $\delta^{18}O$ and temperature, whereas the gray triangle represents their estimate of the average annual values for the same early Eocene river. The open circle is the data point for modern, amount-weighted, average summer (J-J-A) precipitation on Ellesmere Island (from IAEA data). The black "×" symbols are modern, amount-weighted, average annual precipitation $\delta^{18}O$ values and corresponding average annual surface air temperatures from the sites in the global network of the IAEA/WMO (2004). The light gray diamonds represent individual summer months (J-J-A) from northern hemisphere sites in the IAEA/WMO (2004) network. See text.

of Tertiary precipitation may preserve a straightforward response of annual precipitation to warmer annual temperatures (e.g., Dansgaard, 1964; Rozanski et al., 1993). However, the Ax-2 results and the results of Eberle et al. (2010) suggest that the $\delta^{18}O$ values of the Arctic proxies might, instead, be biased toward summer precipitation and its higher $\delta^{18}O$ values.

The question of whether it is annual or seasonal temperature and precipitation $\delta^{18}O$ values that are recorded by the proxies of Fig. 10a can be explored further by plotting the inferred $\delta^{18}O$ values of ancient waters against the corresponding paleotemperatures (Fig. 10b). Fig. 10b also depicts two other data sets: (1) modern annual temperatures and amount-weighted $\delta^{18}O$ values of average annual precipitation from the global network of the IAEA/WMO (2004); and (2) the temperatures and $\delta^{18}O$ values of precipitation for individual summer months (J-J-A) at IAEA sites throughout the northern hemisphere.

With the possible exception of the estimates of Ballantyne et al. (2010a,b), all of the Tertiary results in Fig. 10b have combinations of $\delta^{18}O$ and temperature which are more closely associated with the scatter in the data for modern summer precipitation in the northern hemisphere than with the annual precipitation from any of the globally distributed sample sites. The large-scale spatial relationship between $\delta^{18}O$ values of annual precipitation and temperatures in the early Eocene may have differed somewhat from modern (e.g., Yapp, 2008). However, that proposed Eocene difference is not of sufficient magnitude to account for the observation that the scatter in the data for Tertiary Arctic waters (in three of the four studies) is associated with the scatter in northern hemisphere data for modern *summer* precipitation (Fig. 10b). This affinity is consistent with the idea of a bias toward summer precipitation in those proxy isotopic data. At the same time, the Arctic summer air temperatures were probably warmer than modern (e.g., Elias and Matthews, 2002; Haywood et al., 2009; Eberle et al., 2010).

The evidence for a warmer Arctic climate on land during the Pliocene extends to the Arctic Ocean. Cronin et al. (1993), Knies et al. (2002), and Robinson (2009) present evidence from various marine records, which indicate that the Arctic Ocean was warmer and, at least seasonally, ice-free at about 3.0–3.3 Ma. As suggested by Knies et al. (2002), enhanced contributions of moisture from the Arctic Ocean near the end of the Pliocene could have been an important factor (together with changes in the Earth's obliquity) in the subsequent intensification of northern hemisphere glaciation at the beginning of the Pleistocene (~2.7 Ma). This onset of Pleistocene-style glaciation may have been promoted by decreases in the concentration of tropospheric $CO_2$ from values near 400 ppm to values of ~280 ppm between about 3.2 and 2.8 Ma (e.g., Seki et al., 2010).

At ~4.5 Ma, tropospheric $CO_2$ concentrations seem to have been ~365–415 ppm (Pagani et al., 2009). These concentrations are comparable to the values associated with a warmer Arctic Ocean at ~3.2 Ma. If warmer Arctic Ocean conditions existed in the late Miocene/Pliocene (~5.5–2.8 Ma), evaporation from that warmer ocean could have contributed more water vapor to the air masses over Axel Heiberg and Ellesmere Islands.

Shorter transport distances and smaller temperature differences between oceanic sources of vapor and terrestrial sites of precipitation are generally expected to correlate with more positive $\delta D$ and $\delta^{18}O$ values in precipitation (e.g., Dansgaard, 1964; Friedman et al., 1964; Rozanski et al., 1993). As noted, the results from Ax-2, together with those of Ballantyne et al. (2010a,b), indicate that the $\delta^{18}O$ value of the ambient Pliocene meteoric water was more positive than modern summer precipitation (Fig. 10a and b). Thus, prior to the onset of Pleistocene-style glaciation, water vapor derived from the Arctic Ocean may have played a larger role in the budget of the Arctic hydrologic cycle as far back as ~4–5.5 Ma, and perhaps back to the Eocene (Fig. 10a and b).

### 3.5. $Fe(CO_3)OH$ in Ax-2 goethite

#### *3.5.1. Incremental dehydration–decarbonation*

Results from incremental dehydration–decarbonations of two aliquots of Ax-2 are listed in Table 6 (MHD-2066 and MHD-2331). The $\delta^{13}C$ values of increments of evolved $CO_2$ are plotted in Fig. 11 against the progress variable $X_v(H_2)$. $X_v(H_2)$ is the cumulative hydrogen evolved from the sample as a mole fraction of the total hydrogen in the sample. For dehydration experiment MHD-2066, isothermal vacuum dehydration steps were run at 215 °C, whereas for MHD-2331 the temperature was 173 °C (Table 6).

The rate of breakdown of goethite to hematite in the isothermal vacuum dehydration steps of both experiments was so rapid that $CO_2$ predominantly from the $Fe(CO_3)OH$ component was represented by only one large increment in MHD-2066 and only two consecutive increments in MHD-2331 (Table 6, Fig. 11). Some criteria for assessing which increments of $CO_2$ are robust representatives of the $Fe(CO_3)OH$ component in complex dehydration–decarbonation spectra are discussed in Feng and Yapp (2009). For the two relevant increments of MHD-2331, the amount-weighted average value of $F$ (definition of $F$ in footnote to Table 6) is 0.023 (±0.003) and $\delta^{13}C$ is +6.4 (±0.4)‰, whereas for the single increment of MHD-2066, $F$ is 0.025 (±0.001) and $\delta^{13}C$ is +6.8 (±0.1)‰. Notwithstanding the different temperatures of extraction, the values of F and $\delta^{13}C$ for the $Fe(CO_3)OH$-derived increments of $CO_2$ from MHD-2066 and MHD-2331 are analytically indistinguishable. Such temperature independence is expected for $CO_2$ derived from the $Fe(CO_3)OH$ component, which evolves $CO_2$ only when the enclosing goethite structure breaks down (e.g., Yapp, 1987b; Yapp and Poths, 1991).

The values of F and $\delta^{13}C$ for $Fe(CO_3)OH$, averaged for the two dehydration experiments of Table 6, are 0.024 (±0.003) and +6.6 (±0.5)‰, respectively. This $\delta^{13}C$ value of Ax-2 is plotted in the histogram of Fig. 12 together with published $\delta^{13}C$ values of $Fe(CO_3)OH$ in a variety of goethites. The $\delta^{13}C$ value for Ax-2 is the most positive reported to date from any goethite.

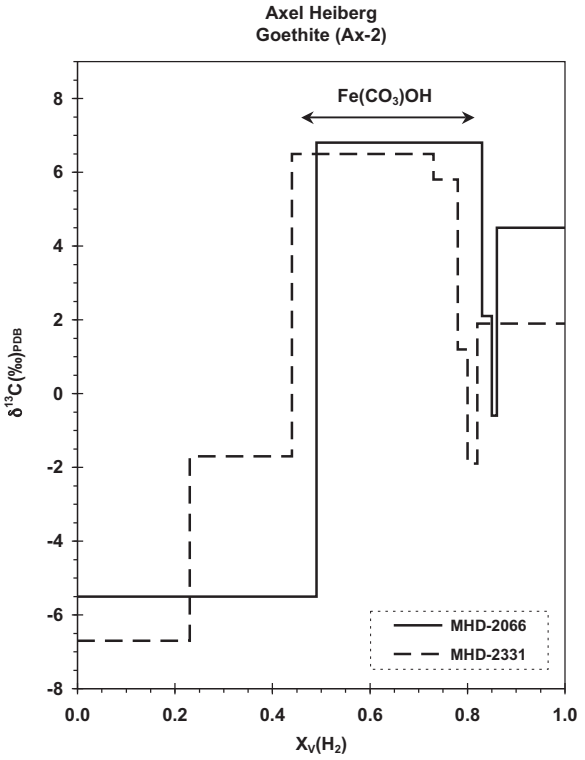


Fig. 11. Incremental dehydration-decarbonation spectra (exclusive of the 100 °C steps) for two aliquots of Ax-2. The labeled arrow indicates the increments which correspond to $CO_2$ evolved from the $Fe(CO_3)OH$ component in solid solution in the goethite (see text and Table 6 for details).

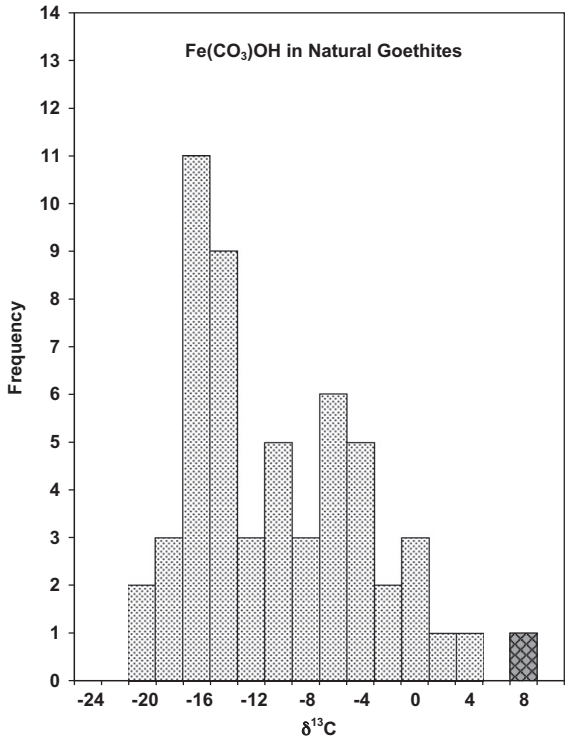


Fig. 12. Histogram of the $\delta^{13}C$ values of the $Fe(CO_3)OH$ component in goethites from a variety of occurrences. The crossed-hatched symbol represents the $\delta^{13}C$ value (+6.6‰) for the $Fe(CO_3)OH$ in Ax-2 goethite. The remaining data are from various sources (Yapp, 2001b; Tabor et al., 2004b; Tabor and Yapp, 2005). Note that the $\delta^{13}C$ value of Ax-2 is more positive than any other goethite value reported to date. See text for discussion.

### 3.5.2. *Paleoenvironmental carbon cycling*

The fact that goethite forms in oxidizing environments (Garrels and Christ, 1965) and that Ax-2 retains the macroscopic aspects of a piece of Eocene wood (i.e., "petrified wood"; Fig. 2a) invites a hypothesis that much of the $CO_2$ present in the ambient environment at the time of goethite crystallization was derived from oxidation of the precursor wood. However, the following items pose problems for this hypothesis: (1) $\delta^{13}C$ values of ~−24‰ were measured for well-preserved Eocene wood from Axel Heiberg Island (e.g., Jahren et al., 2004); and (2) the $\delta^{13}C$ values of $CO_2$ derived from oxidation of such wood are expected to be comparable to the wood. This suggests that the $\delta^{13}C$ value of the $Fe(CO_3)OH$ in the goethite should also be quite negative (Yapp, 1997), but this is not the case for Ax-2. This apparent paradox suggests the need for an alternative hypothesis to explain the very positive $\delta^{13}C$ value of +6.6‰ (Fig. 12).

Jahren et al. (2004) described calcite interspersed with Eocene wood on Axel Heiberg Island and presented evidence that this calcite permineralization occurred in the Eocene soon after burial. They reported $\delta^{13}C$ values of +4.0‰ to +7.4‰ for this calcite. To explain such positive $\delta^{13}C$ values, Jahren et al. (2004) proposed that the Buchanan Lake Formation was buried under reducing conditions in the Eocene and that the calcite crystallized at that time in the presence of $^{13}C$-rich $CO_2$, which was derived predominantly from acetate-fermentation methanogenesis.

Siderite ($FeCO_3$) forms in reducing environments (Garrels and Christ, 1965), and Ludvigson et al. (1998) suggested that methanogenesis could be responsible for the more positive $\delta^{13}C$ values measured in sphaerosiderites. Ufnar et al. (2002) compiled data which included sphaerosiderites from the north slope of Alaska with some $\delta^{13}C$ values >+10‰. If a reducing Eocene burial environment on Axel Heiberg Island led to mobilization of $Fe^{2+}$ and, in some instances, to local crystallization of siderite (replacing the wood), that siderite would have formed in the presence of the $^{13}C$-rich $CO_2$ associated with methanogenesis. As a result, such siderite would be expected to have positive $\delta^{13}C$ values (similar to the calcite values measured by Jahren et al., 2004).

Oxidative weathering of siderite to produce goethite is illustrated by the following reaction:

$$4FeCO_3 + O_2 + 2H_2O \rightarrow 4FeOOH + 4CO_2 \quad (9)$$

In the water-dominated microenvironments of the interfaces where oxidation of siderite and nucleation and growth of goethite occur, $CO_2$ derived from the siderite could be expected to be the overwhelming local source of $CO_2$ and should dominate the carbon isotope budget. If the hypothesized siderite precursor did form in the same methanogenic Eocene burial environment as the $^{13}C$-rich calcites analyzed by Jahren et al. (2004), Eq. (9) indicates that the carbon isotope composition (+6.6‰) of the $Fe(CO_3)OH$ component

in the goethite of Ax-2 could be a relic of that Eocene environment. Note that the value of +6.6‰ is within the range of calcite $\delta^{13}C$ values measured by Jahren et al. (2004). Thus, in this carbon isotopic sense, the goethite, which is a product of an oxidizing late Miocene–Pliocene environment, contains a "memory" of an Eocene methanogenic burial environment in the host middle Eocene paleosol.

The siderite oxidation scenario explains the seemingly contradictory observations of (1) a petrified-wood texture for Ax-2 and (2) a very positive $\delta^{13}C$ value (+6.6‰) for $Fe(CO_3)OH$ in the goethite (not the very negative value expected if oxidizing wood had been the local source of $CO_2$). This hypothesis also has the merit of accounting for (3) mobilization of iron (in a reducing environment), then (4) concentration of iron (localized siderite precipitation), followed by (5) late Miocene/Pliocene oxidation with formation of the Al-free, comparatively large, coherent sample of Ax-2 goethite.

The mole fraction ($X$) of $Fe(CO_3)OH$ in Ax-2 goethite is 0.012 (±0.002), where $X = 0.5$ F (Yapp and Poths, 1993). For this value of $X$ and a temperature of 3 °C, the Henry's Law equation of Yapp and Poths (1992) indicates that the concentration of ambient subsurface $CO_2$ at the time of goethite crystallization was about 27,000 ppmV. However, because the $^{13}C$-rich $CO_2$ from an in situ source constituted a "third component" in the subsurface $CO_2$ mixture, it precluded use of the measured values of X and $\delta^{13}C$ in Ax-2 goethite to determine the concentration of $CO_2$ in the latest Miocene/Pliocene troposphere (Yapp, 2001b, 2002). A less extreme positive shift was found in the $\delta^{13}C$ values of diagenetic goethite hosted by a mid-paleolatitude Cretaceous laterite (Feng and Yapp, 2009). That shift was also attributed to a relatively $^{13}C$-rich, third component derived from oxidation of siderite that had crystallized in an older diagenetic event.

The Ax-2 goethite of the current study and the goethite of Feng and Yapp (2009) were hosted by paleosols that were stratigraphically associated with coal deposits (i.e., electron donor, reducing agents). If an iron-bearing paleosol in such a stratigraphic context experienced two temporally distinct diagenetic events, the first reducing and the second oxidizing (yielding goethite), the forgoing hypothesis suggests that high values of $X$ coupled with unexpectedly high $\delta^{13}C$ values for the $Fe(CO_3)OH$ component in goethite could indicate a diagenetic origin for the goethite. The $^{13}C$-rich carbon in the $Fe(CO_3)OH$ would be derived from precursor carbonate that formed in the older, reducing, presumably methanogenic environment. However, $\delta^{13}C$ values from a single sample may not, by themselves, distinguish such diagenetic goethite from pedogenic goethite that preserves information on a three-component $CO_2$ system that could originally have been present in some soils (Hsieh and Yapp, 1999).

## 4. CONCLUSIONS

An apparent carbon isotope paradox inherent in a measured $\delta^{13}C$ value of +6.6‰ for the $Fe(CO_3)OH$ component in late Miocene/Pliocene (~5.5–2.8 Ma) Ax-2 goethite from Axel Heiberg Island at ~80°N latitude (which constitutes a sample of "petrified wood") is resolved if the $Fe(CO_3)OH$ component retains a carbon isotope "memory" of a precursor carbonate (possibly siderite) that initially replaced the wood in a methanogenic, middle Eocene, diagenetic environment. Thus, the Ax-2 goethite appears to retain different types of information about the environments of two distinctly different diagenetic redox systems that were separated in time by about 40 million years.

In combination, the paleotemperatures and $\delta^{18}O$ values of ancient waters (from Ax-2 and published results from three Eocene or Pliocene proxy sites on Axel Heiberg and Ellesmere Islands) are consistent with a warm season bias in those isotopic proxies. The results are also consistent with higher proportions of J-J-A precipitation in the annual total. If so, this emphasizes the importance of seasonality at high latitudes even in times of warmer global climates, and suggests that the Arctic hydrologic cycle, as expressed in the seasonal distribution and isotopic composition of precipitation (perhaps modified by a warmer Arctic Ocean), differed from modern.

The results of the current study show that useful paleoenvironmental (including climatic) information can be obtained from diagenetic goethite, when measurements of the stable isotope ratios of hydrogen, oxygen, and carbon are combined with the determination of credible (U–Th)/He ages for the same sample.

## ACKNOWLEDGMENTS

We thank Dr. Hope Jahren for providing the sample of Ax-2 and Dr. Weimin Feng for assistance with the hydrogen and some of the carbon isotope analyses. The paper benefited from the comments and reviews of Hope Jahren, Derek Sjostrom, and an anonymous reviewer. This research was supported by NSF grant EAR-0616627 to C.J.Y. D.L.S. acknowledges the Ann and Gordon Getty Foundation.

## REFERENCES

Ballantyne A. P., Rybczynski N., Baker P. A., Harington C. R. and White D. (2006) Pliocene Arctic temperature constraints from the growth rings and isotopic composition of fossil larch. *Palaeogeogr. Palaeoclimatol. Palaeoecol.* **242**, 188–200.

Ballantyne A. P., Greenwood D. R., Sinninghe Damsté J. S., Csank A. Z., Eberle J. J. and Rybczynski N. (2010a) Significantly warmer Arctic surface temperatures during the Pliocene indicated by multiple independent proxies. *Geology* **38**, 603–606.

Ballantyne A. P., Greenwood D. R., Sinninghe Damsté J. S., Csank A. Z., Eberle J. J. and Rybczynski N. (2010b) Significantly warmer Arctic surface temperatures during the Pliocene indicated by multiple independent proxies. *Geology* **38**, 603–606 (supplemental information, GSA Data Repository item 2010165, www.geosociety.org/pubs/ft2010.htm).

Bao H., Koch P. L. and Thiemens M. H. (2000) Oxygen isotope composition of ferric oxides from recent soil, hydrologic, and marine environments. *Geochim. Cosmochim. Acta* **64**, 2221–2231.

Bird M. I., Longstaffe F. J., Fyfe W. S. and Bildgen P. (1992) Oxygen isotope systematics in a multi-phase weathering system in Haiti. *Geochim. Cosmochim. Acta* **56**, 2831–2838.

Bird M. I., Longstaffe F. J., Fyfe W. S., Kronberg B. I. and Kishida A. (1993) An oxygen-isotope study of weathering in the eastern

Amazon Basin, Brazil. *Geophys. Monogr.* **78**, 295–307 (Climate Change in Continental Isotopic Records).

Boily J.-F., Szanyi J. and Felmy A. R. (2006) A combined FTIR and TPD study on the bulk and surface dehydroxylation and decarbonation of synthetic goethite. *Geochim. Cosmochim. Acta* **70**, 3613–3624.

Carslaw H. S. and Jaeger J. C. (1959) *Conduction of Heat in Solids*, second ed. Oxford University Press, Oxford, 510 pp.

Clayton R. N. and Mayeda T. K. (1963) The use of bromine pentafluoride in the extraction of oxygen from oxides and silicates for isotopic analysis. *Geochim. Cosmochim. Acta* **27**, 43–52.

Craig H. (1961) Isotopic variations in meteoric waters. *Science* **133**, 1702–1703.

Cronin T. M., Whatley R., Wood A., Tsukagoshi A., Ikeya N., Brouwers E. M. and Briggs, Jr., W. M. (1993) Microfaunal evidence for elevated Pliocene temperatures in the Arctic Ocean. *Paleoceanography* **8**, 161–173.

Dansgaard W. (1964) Stable isotopes in precipitation. *Tellus* **16**, 436–468.

Dideriksen K., Christiansen B. C., Frandsen C., Balic-Zunic T., Mørup S. and Stipp S. L. S. (2010) Paleo-redox boundaries in fractured granite. *Geochim. Cosmochim. Acta* **74**, 2866–2880.

Eberle J. J., Fricke H. C., Humphrey J. D., Hackett L., Newbrey M. G. and Hutchison J. H. (2010) Seasonal variability in Arctic temperatures during early Eocene time. *Earth Planet. Sci. Lett.* **296**, 481–486.

Elias S. A. and Matthews, Jr., J. V. (2002) Arctic North American seasonal temperatures from the latest Miocene to the Early Pleistocene, based on mutual climatic range analysis of fossil beetle assemblages. *Can. J. Earth Sci.* **39**, 911–920.

Feng W. and Yapp C. J. (2008) Experimental tests of the effects of Al substitution on the goethite-water D/H fractionation factor. *Geochim. Cosmochim. Acta* **72**, 1295–1311.

Feng W. and Yapp C. J. (2009) Paleoenvironmental implications of concentration and $^{13}C/^{12}C$ ratios of $Fe(CO_3)OH$ in goethite from a mid-latitude Cenomanian laterite in southwestern Minnesota. *Geochim. Cosmochim. Acta* **73**, 2559–2580.

Fifarek R. H. and Rye R. O. (2005) Stable-isotope geochemistry of the Pierina high-sulfidation Au–Ag deposit, Peru: influence of hydrodynamics on $SO_4^{2-}$–$H_2S$ sulfur isotopic exchange in magmatic-steam and steam-heated environments. *Chem. Geol.* **215**, 253–279.

Friedman I., Redfield A. C., Schoen B. and Harris J. (1964) The variation of the deuterium content of natural waters in the hydrologic cycle. *Rev. Geophys.* **2**, 177–224.

Garrels R. M. and Christ C. L. (1965) *Solutions, Minerals, and Equilibria*. Harper and Row, New York, 450 pp.

Girard J. P., Razanadranorosa D. and Freyssinet P. (1997) Laser oxygen isotope analysis of weathering goethite from the lateritic profile of Yaou, French Guiana: paleoweathering and paleoclimatic implications. *Appl. Geochem.* **12**, 163–174.

Girard J. P., Freyssinet P. and Gilles C. (2000) Unraveling climatic change from intra-profile variation in oxygen and hydrogen isotopic composition of goethite and kaolinite in laterites: an integrated study from Yaou, French Guiana. *Geochim. Cosmochim. Acta* **64**, 4467–4477.

Girard J.-P., Freyssinet P. and Morillon A.-C. (2002) Oxygen isotope study of Cayenne duricrust paleosurfaces: implications for past climate and laterization processes over French Guiana. *Chem. Geol.* **191**, 329–343.

Grosz S., Matthews A., Ilani S., Ayalon A. and Garfunkel Z. (2006) Iron mineralization and dolomitization in the Paran Fault zone, Israel: implications for low-temperature basinal fluid processes near the Dead Sea Transform. *Geofluids* **6**, 137–153.

Harrison J. C., Mayr U., McNeil D. H., Sweet A. R., McIntyre D. J., Eberle J. J., Harington C. R., Chalmers J. A., Dam G. and Nøhr-Hansen H. (1999) Correlation of the Cenozoic sequences of the Canadian Arctic region and Greenland; implications for the tectonic history of northern North America. *Bull. Can. Petrol. Geol.* **47**, 223–254.

Haywood A. M., Chandler M. A., Valdes P. J., Salzmann U., Lunt D. J. and Dowsett H. J. (2009) Comparison of mid-Pliocene climate predictions produced by the HadAM3 and GCMAM3 General Circulation Models. *Global Planet. Change* **66**, 208–224.

Heim J. A., Vasconcelos P. M., Shuster D. L., Farley K. A. and Broadbent G. (2006) Dating paleochannel iron ore by (U–Th)/He analysis of supergene goethite, Hamersley province, Australia. *Geology* **34**, 173–176.

Hein J. R., Yeh H. W., Gunn S. H., Gibbs A. E. and Wang C. H. (1994) Composition and origin of hydrothermal ironstones from central Pacific seamounts. *Geochim. Cosmochim. Acta* **58**, 179–189.

Hsieh J. C. C. and Yapp C. J. (1999) Stable carbon isotope budget of $CO_2$ in a wet, modern soil as inferred from $Fe(CO_3)OH$ in pedogenic goethite: possible role of calcite dissolution. *Geochim. Cosmochim. Acta* **63**, 767–783.

Hren M. T., Lowe D. R., Tice M. M., Byerly G. and Chamberlain C. P. (2006) Stable isotope and rare earth element evidence for recent ironstone pods within Archean Barberton greenstone belt, South Africa. *Geochim. Cosmochim. Acta* **70**, 1457–1470.

IAEA/WMO (2004) Global Network of Isotopes in Precipitation. The GNIP Database. Accessible at: <http://isohis.iaea.org>.

Jahren A. H. (2007) The Arctic forest of the middle Eocene. *Annu. Rev. Earth Planet. Sci.* **35**, 509–540.

Jahren A. H. and Sternberg L. S. L. (2002) Eocene meridional weather patterns reflected in the oxygen isotopes of Arctic fossil wood. *GSA Today* **1**, 4–9.

Jahren A. H. and Sternberg L. S. L. (2003) Humidity estimate for the middle Eocene Arctic rain forest. *Geology* **31**, 463–466.

Jahren A. H. and Sternberg L. S. L. (2008) Annual patterns within tree rings of the ASrctic middle Eocene (ca. 45 Ma): isotopic signatures of precipitation, relative humidity, and deciduousness. *Geology* **36**, 99–102.

Jahren A. H., LePage B. A. and Werts S. P. (2004) Methanogenesis in Eocene Arctic soils inferred from $\delta^{13}C$ of tree fossil carbonates. *Palaeogeogr. Palaeoclimatol. Palaeoecol.* **214**, 34–358.

Jahren A. H., Byrne M. C., Graham H. V., Sternberg L. S. L. and Summons R. E. (2009) The environmental water of the middle Eocene Arctic: evidence from $\delta D$, $\delta^{18}O$ and $\delta^{13}C$ within specific compounds. *Palaeogeogr. Palaeoclimatol. Palaeoecol.* **271**, 96–103.

Johnsen S. J., Dahl-Jensen D., Gundestrup N., Steffensen J. P., Clausen H. B., Miller H., Masson-Delmotte V., Sveinbjörnsdottir A. E. and White J. (2001) Oxygen isotope and palaeotemperature records from six Greenland ice-core stations: Camp Century, Dye-3, GRIP, GISP2, Renland and NorthGRIP. *J. Quatern. Sci.* **16**, 299–307.

Jury W. A., Gardner W. R. and Gardner W. H. (1991) *Soil Physics*. Wiley, New York, 328 pp.

Knies J., Matthiessen J., Vogt C. and Stein R. (2002) Evidence of 'Mid-Pliocene (13 Ma) global warmth' in the eastern Arctic Ocean and implications for the Svalbard/Barents Sea ice sheet during the late Pliocene and early Pleistocene (3–1.7 Ma). *Boreas* **31**, 82–93.

Lambert F., Delmonte B., Petit J. R., Bigler M., Kaufmann P. R., Hutterl M. A., Stocker T. F., Ruth U. J. P., Steffensen J. P. and Maggi V. (2008) Dust-climate couplings over the past 800,000 years from the EPICA Dome C ice core. *Nature* **452**, 616–619.

Langmuir D. (1978) Uranium solution-mineral equilibria at low temperatures with applications to sedimentary ore deposits. *Geochim. Cosmochim. Acta* **42**, 547–569.

Lippolt H. J., Brander T. and Mankopf N. R. (1998) An attempt to determine formation ages of goethites and limonites by (U + Th)-$^4$He dating. *Neues Jb. Mineral. Monat.* **11**, 505–528.

Ludvigson G. A., González L. A., Metzger R. A., Witzke B. J., Brenner R. L., Murillo A. P. and White T. S. (1998) Meteoric sphaerosiderite lines and their use for paleohydrology and paleoclimatology. *Geology* **26**, 1039–1042.

Lugowski A., Ogg J. and Gradstein F. (2009) TSCreator visualization of enhanced Geologic Time Scale 2004 database (Version 4.2). Available from: <http://www.tscreator.org>.

Neck V., Altmaier M., Müller R., Bauer A., Fanghänel Th. and Kim J. I. (2003) Solubility of crystalline thorium. *Radiochim. Acta* **91**, 253–262.

Pack A., Gutzmer J., Beukes N. J. and Van Niekerk H. S. (2000) Supergene ferromanganese wad deposits derived from Permian Karoo strata along the Late Cretaceous-Mid-Tertiary African land surface, Ryedale, South Africa. *Econ. Geol.* **95**, 203–220.

Pagani M., Liu Z., LaRiviere J. and Ravelo A. C. (2009) Earth system climate sensitivity determined from Pliocene carbon dioxide concentrations. *Nat. Geosci.* doi:10.1038/NGEO724.

Poage M. A., Sjostrom D. J., Goldberg J., Chamberlain C. P. and Furniss G. (2000) Isotopic evidence for Holocene climate change in the northern Rockies from a goethite-rich ferricrete chronosequence. *Chem. Geol.* **166**, 327–340.

Rai D., Moore D. A., Oakes C. S. and Yui M. (2000) Thermodynamic model for the solubility of thorium dioxide in the $Na^+$–$Cl^-$–$OH^-$–$H_2O$ system at 23 °C and 90 °C. *Radiochim. Acta* **88**, 297–306.

Robinson M. M. (2009) New quantitative evidence of extreme warmth in the Pliocene Arctic. *Stratigraphy* **6**, 265–275.

Rozanski K., Araguas-Araguas L. and Gonfiantini R. (1993) Isotopic patterns in modern global precipitation. *Geophys. Monogr.* **78**, 1–36 (Climate Change in Continental Isotopic Records).

Savin S. and Epstein S. (1970) The oxygen and hydrogen isotope geochemistry of clay minerals. *Geochim. Cosmochim. Acta* **34**, 25–42.

Schulze D. G. (1984) The influence of aluminum on iron oxides. VIII. Unit cell dimensions of Al-substituted goethites and estimation of Al from them. *Clays Clay Mineral.* **32**, 36–44.

Schwertmann U. (1988) Occurrence and formation of iron oxides in various pedoenvironments. In *Iron in Soils and Clay Minerals* (eds. J. W. Stucki, B. A. Goodman and U. Schwertmann). Reidel, Dordrecht, pp. 267–308.

Seidel M., Pack A., Sharp Z. D. and Seidel E. (2005) The Kakopetros and Ravdoucha iron-oxide deposits, western Crete, Greece. Fluid transport and mineralization within a detachment zone. *Econ. Geol.* **100**, 165–174.

Seki O., Foster G. L., Schmidt D. N., Mackensen A., Kawamura K. and Pancost R. D. (2010) Alkenone and boron-based $pCO_2$ records. *Earth Planet. Sci. Lett.* **292**, 201–211.

Sherman D. M., Peacock C. L. and Hubbard C. G. (2008) Surface complexation of U(VI) on goethite (α-FeOOH). *Geochim. Cosmochim. Acta* **72**, 298–310.

Shuster D. L. and Farley K. A. (2004) $^4$He/$^3$He thermochronometry. *Earth Planet. Sci. Lett.* **217**, 1–17.

Shuster D. L. and Farley K. A. (2005) $^4$He/$^3$He thermochronometry: theory, practice, and potential complications. *Rev. Mineral. Geochem.* **58**, 181–203.

Shuster D. L., Vasconcelos P. M., Heim J. A. and Farley K. A. (2005) Weathering geochronology by (U–Th)/He dating of goethite. *Geochim. Cosmochim. Acta* **69**, 659–673.

Sjostrom D. J., Hren M. T. and Chamberlain C. P. (2004) Oxygen isotope records of goethite from ferricrete deposits indicate regionally varying Holocene climate change in the Rocky Mountain region, USA. *Quatern. Res.* **61**, 64–71.

Tabor N. J. (2007) Permo-Pennsylvanian palaeotemperatures from Fe-Oxide and phyllosilicate $\delta^{18}O$ values. *Earth Planet. Sci. Lett.* **253**, 159–171.

Tabor N. J. and Yapp C. J. (2005) Juxtaposed Permian and Pleistocene isotopic archives: surficial environments recorded in calcite and goethite from the Wichita Mountains, Oklahoma. In *Isotopic and Elemental Tracers of Cenozoic Climate Change* (eds. G. Mora and D. Surge). GSA Spec. Pap. 395, pp. 55–70.

Tabor N. J., Montañez I. P., Zierenberg R. and Currie B. S. (2004a) Mineralogical and geochemical evolution of a basalt-hosted fossil soil (Late Triassic, Ischigualasto Formation, northwest Argentina): potential for paleoenvironmental reconstruction. *GSA Bull.* **116**, 1280–1293.

Tabor N. J., Yapp C. J. and Montañez I. P. (2004b) Goethite, calcite, and organic matter from Permian and Triassic soils: carbon isotopes and $CO_2$ concentrations. *Geochim. Cosmochim. Acta* **68**, 1503–1517.

Ufnar D. F., González L. A., Ludvigson G. A., Brenner R. L. and Witzke B. L. (2002) The mid-Cretaceous water bearer: isotope mass balance quantification of the Albian hydrologic cycle. *Palaeogeogr. Palaeoclimatol. Palaeoecol.* **188**, 51–71.

Wolf R. A., Farley K. A. and Kass D. M. (1998) Modeling of the temperature sensitivity of the apatite (U–Th)/He thermochronometer. *Chem. Geol.* **148**, 105–114.

Yapp C. J. (1987a) Oxygen and hydrogen isotope variations among goethites (a-FeOOH) and the determination of paleotemperatures. *Geochim. Cosmochim. Acta* **51**, 355–364.

Yapp C. J. (1987b) A possible goethite-iron (III) carbonate solid solution and the determination of $CO_2$ partial pressures in low temperature geologic systems. *Chem. Geol.* **64**, 259–268.

Yapp C. J. (1990) Oxygen isotopes in iron (III) oxides. 1. Mineral–water fractionation factors. *Chem. Geol.* **85**, 329–335.

Yapp C. J. (1993) Paleoenvironment and the oxygen isotope geochemistry of ironstone of the Upper Ordovician Neda Formation, Wisconsin, USA. *Geochim. Cosmochim. Acta* **57**, 2319–2327.

Yapp C. J. (1997) An assessment of isotopic equilibrium in goethites from a bog iron deposit and a lateritic regolith. *Chem. Geol.* **135**, 159–171.

Yapp C. J. (1998) Paleoenvironmental interpretations of oxygen isotope ratios in oolitic ironstones. *Geochim. Cosmochim Acta* **62**, 2409–2420.

Yapp C. J. (2000) Climatic implications of surface domains in arrays of δD and $\delta^{18}O$ from hydroxyl minerals: goethite as an example. *Geochim. Cosmochim. Acta* **64**, 2009–2025.

Yapp C. J. (2001a) Rusty relics of Earth history: iron (III) oxides, isotopes and surficial environments. *Ann. Rev. Earth Planet. Sci.* **29**, 165–199.

Yapp C. J. (2001b) Mixing of $CO_2$ in surficial environments as recorded by the concentration and $\delta^{13}C$ values of the $Fe(CO_3)OH$ component in goethite. *Geochim. Cosmochim. Acta* **65**, 4115–4130.

Yapp C. J. (2002) Erratum to Crayton J. Yapp (2001), "Mixing of $CO_2$ in surficial environments as recorded by the concentration and $\delta^{13}C$ values of the $Fe(CO_3)OH$ component in goethite", GCA, Vol. 65, 4115–4130. *Geochim. Cosmochim. Acta* **66**, 1497.

Yapp C. J. (2007) Oxygen isotopes in synthetic goethite and a model for the apparent pH dependence of goethite-water $^{18}O/^{16}O$ fractionation. *Geochim. Cosmochim. Acta* **71**, 1115–1129.

Yapp C. J. (2008) $^{18}O/^{16}O$ and D/H in goethite from a North American Oxisol of the Early Eocene climatic optimum. *Geochim. Cosmochim. Acta* **72**, 5838–5851.

Yapp C. J. and Pedley M. D. (1985) Stable hydrogen isotopes in iron oxides-II. D/H variations among natural goethites. *Geochim. Cosmochim. Acta* **49**, 487–495.

Yapp C. J. and Poths H. (1990) Infrared spectral evidence for a minor Fe(III) carbonate-bearing component in natural goethite. *Clays Clay Mineral.* **38**, 442–444.

Yapp C. J. and Poths H. (1991) $^{13}C/^{12}C$ ratios of the Fe(III) carbonate component in natural goethites. In *Stable Isotope Geochemistry: A Tribute to Samuel Epstein* (eds. H. P. Taylor Jr., J. R. O'Neil and I. R. Kaplan). Geochem. Soc. Spec. Publ. **3**, pp. 257–270.

Yapp C. J. and Poths H. (1992) Ancient atmospheric $CO_2$ pressures inferred from natural goethites. *Nature* **355**, 342–344.

Yapp C. J. and Poths H. (1993) The carbon isotope geochemistry of goethite (alpha-FeOOH) in ironstone of the Upper Ordovician Neda Formation, Wisconsin, USA: implications for early Paleozoic continental environments. *Geochim. Cosmochim. Acta* **57**, 2599–2611.

Yapp C. J. and Poths H. (1995) Stable hydrogen isotopes in iron oxides: III. Nonstoichiometric hydrogen in goethite. *Geochim. Cosmochim. Acta* **59**, 3405–3412.

*Associate editor:* James Farquhar